5-11-2009

Blind Synchronization and Detection of Nyquist Pulse Shaped QAM Signals

Evren Terzi
University of South Florida

Blind Synchronization and Detection of

Nyquist Pulse Shaped QAM Signals

by

Evren Terzi

A thesis submitted in partial fulfillment
of the requirements for the degree of
Master of Science in Electrical Engineering
Department of Electrical Engineering
College of Engineering
University of South Florida

Major Professor: Huseyin Arslan, Ph.D.
Wilfrido Moreno, Ph.D.
Paris H.Wiley, Ph.D.

Date of Approval:
May 11, 2009

Keywords: symbol rate, baud rate, frequency offset, phase offset, modulation identification

DEDICATION

To my parents.

ACKNOWLEDGEMENTS

First, I would like to thank my advisor, Dr. Huseyin Arslan for his guidance and encouragement throughout the course of this thesis. His professionalism and discipline has been very inspiring for me. I have to thank him for his patience throughout the development of this thesis and his precious advices.

I would like to thank to Dr. Wilfrido Moreno and Dr. Paris H. Wiley for serving in my committee and for their valuable feedback and suggestions.

I wish to thank to all my friends at USF. I would like to thank to the past and present members of wireless communications and signal processing (WCSP) group; Sabih Guzelgoz, Dr. Celal Ceken, Dr. Hasari Celebi, Dr. Tevfik Yucek, Dr. Hisham A. Mahmoud, Mustafa E. Sahin, Serhan Yarkan, Ali Gorcin, Ozgur Yurur, Hasan B. Celebi, Ali Riza Ekti, Ibrahim Demirdogen, Omar Zakaria, A. Cagatay Talay, Bahattin Karakaya, Mustafa C. Erturk and Sadia Ahmed for their fruitful discussions.

I also would like to thank to my dear friends Osman Murat, Mert Dogan, Can Arkun and Tolga Yildirim for their continuous encouragement and support during the development of this thesis.

Last but by no means least, I would like to thank my parents, to my sisters and to my brother, for their continued support, encouragement and love. I would not achieve this success without them.

TABLE OF CONTENTS

LIST OF TABLES iii

LIST OF FIGURES iv

ABSTRACT vi

CHAPTER 1 INTRODUCTION 1
1.1. Organization of Thesis 3

CHAPTER 2 BANDWIDTH AND CARRIER FREQUENCY ESTIMATION 5
2.1. Introduction 5
2.2. Bandwidth Estimation 5
2.2.1. Literature Overview and Challenges 6
2.2.2. Method Proposed 6
2.2.3. Simulation Results 8
2.3. Carrier Frequency Estimation 9
2.3.1. Literature Overview and Challenges 9
2.3.2. Method Proposed 9
2.3.3. Simulation Results 11

CHAPTER 3 SYMBOL RATE ESTIMATION 13
3.1. Introduction 13
3.2. Literature Overview and Challenges 14
3.3. Method Proposed 18
3.4. Simulation Results 22

CHAPTER 4 PULSE SHAPE AND OPTIMAL SAMPLING PHASE ESTIMATION 26
4.1. Introduction 26
4.2. Nyquist Criterion 27
4.3. Pulse Shape Estimation 28
4.3.1. Literature Overview and Challenges 28
4.3.2. Method Proposed 30
4.4. Optimum Sampling Instant Estimation 33
4.4.1. Challenges 33
4.4.2. Method Proposed 37
4.5. Simulation Results 37

CHAPTER 5 MODULATION IDENTIFICATION, FREQUENCY OFFSET AND PHASE OFFSET ESTIMATION AND CORRECTION 40
5.1. Introduction 40
5.1.1. Literature Overview and Challenges for Frequency Offset and Phase Offset 45
5.1.2. Literature Overview and Challenges for Modulation Identification 50
5.2. Method Proposed 52
5.3. Simulation Results 59

CHAPTER 6 SUMMARY AND CONCLUSIONS 66
6.1. Contributions 66
6.2. Conclusions 67

REFERENCES 68

LIST OF TABLES

Table 1: SNR vs. False Alarm Rate 39

Table 2: False Alarm Rate of Modulation Identification Technique Proposed 61

LIST OF FIGURES

Figure 1: Block Diagram of a Blind Receiver 2

Figure 2: Bandwidth Estimation 8

Figure 3: Carrier Frequency Representation 11

Figure 4: Carrier Frequency Estimation Error 12

Figure 5: Block Diagram of Symbol Rate Estimation – Coarse Estimation, Fine Estimation and Timing Recovery 13

Figure 6: Block Diagram of Proposed Symbol Rate Estimation Method 18

Figure 7: Representation of Polynomial Fitting 19

Figure 8: Effect of Excess Bandwidth on Spectral Line Generation for Cyclic Correlation Based Algorithms 21

Figure 9: Coarse Estimation Part of Proposed Method 23

Figure 10: RMSE Performance of Proposed Method Compared to [7] 24

Figure 11: Success Rate of Proposed Method Compared to [7] 25

Figure 12: A Raised Cosine Pulse 30

Figure 13: Eye Diagram of In-Phase Component of a 4QAM Signal – Perfect Matched Filtering 32

Figure 14: Eye Diagram of In-Phase Component of a 4QAM Signal - Wrong Matched Filtering (Transmitter Roll-off Factor = 0.35 – Receiver Roll-off Factor = 0.50) 32

Figure 15: Eye Diagram of In-Phase Component of a 4QAM Signal - No Matched Filtering 33

Figure 16: Downsampled BPSK Signal with 11 Sample Errors from the Optimum Sampling Instant 34

Figure 17: Downsampled BPSK Signal at Optimum Sampling Instant 34

Figure 18: Optimum Sampling Instant for a 16QAM Signal 36

Figure 19: RMSE Performance with Various Excess Bandwidth Conditions 38

Figure 20: A 64QAM Constellation Affected only by Phase Offset 41

Figure 21: Constellations Diagram after Downsampling 42

Figure 22: Different 16QAM Constellations 43

Figure 23: Different 16QAM Constellations with Frequency Offset 44

Figure 24: Probability Density Function of the Rectangular 16QAM Constellation 45

Figure 25: Proposed Method 53

Figure 26: Joint Phase and Frequency Offset Correction 55

Figure 27: 16QAM Signal with a Positive Frequency Offset 56

Figure 28: Phase Rotation Tracking 57

Figure 29: Constellation Diagram after Mapping all Symbols to the First Quadrant 58

Figure 30: Representation of Threshold Value 59

Figure 31: Useful Constellations of 32QAM 60

Figure 32: Frequency Offset and Phase Rotation Tracking for 16QAM 62

Figure 33: Constellation Diagram of a 16QAM Signal after Frequency Offset Correction 63

Figure 34: Frequency Offset and Phase Rotation Tracking for 64QAM 64

Figure 35: Constellation Diagram of a 64QAM Signal after Frequency Offset Correction 65

BLIND SYNCHRONIZATION AND DETECTION OF

NYQUIST PULSE SHAPED QAM SIGNALS

Evren Terzi

ABSTRACT

This thesis proposes a blind receiver for the Nyquist pulse shaped quadrature-amplitude modulation (QAM) signals. The focus is on single carrier signals. The blind receiver includes the estimation of the symbol rate, the roll-off factor of the filter, the optimal sample phase, the frequency offset, the phase offset and as well as the correction of frequency and phase offsets.

The blind receiver is proposed for the cognitive radio applications. Cognitive radios are intelligent devices which can adapt themselves according to its user and its environment, i.e. they are aware of the user and the environment. Another importance of cognitive radios is they can detect the incoming signal and demodulate it and also respond to the transmitting node with the same parameters. In order to demodulate the signal and to respond the transmitter node, there are some parameters which are needed to be known.

The estimation starts with the bandwidth and carrier frequency, continued by the estimation of the symbol rate, which is a crucial factor. After the estimation and

restrictions of these parameters, the roll-off factor of the filter is estimated for match filtering to remove the inter symbol interference (ISI) effect. Then the optimal sample phase is detected and the signal is downsampled. The following procedures include the modulation identification and estimation and correction of both frequency and phase offsets.

The estimation algorithms performance is compared to the performances of the other algorithms available in the literature. These simulation results are presented and discussed in this thesis.

CHAPTER 1

INTRODUCTION

As technology evolves, the wireless communications industry is going towards to evolving cognitive radio applications. Cognitive radio is basically an intelligent wireless device which is aware of the environment, spectrum, location, RF environment, power, user, spectrum etc.

Cognitive radios prevent spectral crowding by using the spectrum intelligently. They can detect the empty chunks in the spectrum and they can switch to that carrier frequency easily and act as a secondary user. Another important feature of cognitive radios is that they can detect the incoming signal and demodulate it. This feature of cognitive radios highlights the importance of blind demodulation. By extracting the signal information, it can respond to the source radio using the same parameters. This feature is called co-existence. Another important result of being able to demodulate the signal is that it can understand the radio being used at the transmitter and according to the properties of the radio at the transmitter, and it can use the empty frequency bins [1, 2].

Another area where cognitive radios are very important is public safety applications. After disasters, the communication network becomes very congested and it is very hard for safety officers, i.e. policeman, fireman and medical teams, to communicate with each other. This situation worsens the effect of the disaster. As mentioned above, the robustness of cognitive radios to the spectral crowding problem is

an important feature that makes cognitive radios important. Again, in these kinds of situations, being able to demodulate the incoming signal for a safety officer is very important. The signal parameters of the transmitter node are unknown. The cognitive radio needs to detect the parameters of the incoming signal and must be able to demodulate it. The importance of blind receivers rises at this point in cognitive radio and public safety applications.

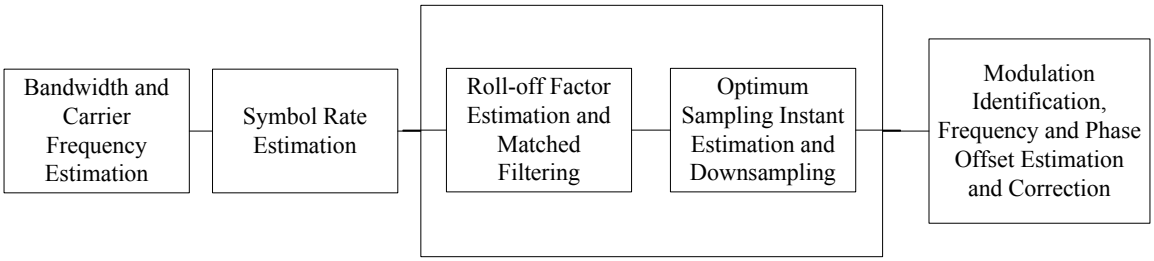

Figure 1: Block Diagram of a Blind Receiver

A block diagram of a blind receiver can be found in Figure 1. In blind receivers there is no a priori information about the signal and they are referred as non-data aided receivers. Non-data aided means that there is no pilot sequence used for channel estimation or synchronization to the signal and there is no bandwidth occupied for the transmission of pilots which is desirable. The signal is received at the receiver and all related parameters extracted. Bandwidth estimation is the first step for blind receivers and it creates some room for the symbol rate estimation. After the bandwidth carrier frequency is estimated, the signal is downshifted to baseband for processing. The accuracy of carrier frequency estimation is very important because the wrong carrier synchronization will cause frequency offsets. The estimation of carrier frequency depends on the bandwidth. The most crucial parameter for a blind receiver is the symbol rate. Most of the remaining blocks, such as pulse shape estimation and optimum sampling

phase estimation, depend on the symbol rate. While obtaining the symbol rate, the oversampling rate is also determined. The pulse shape and optimum sampling instant estimations follow the symbol rate estimation. The symbol rate and oversampling rate information is used in this step to find the roll-off factor of the filter used and the sampling instant where the signal is sampled. When the roll-off factor of the filter is determined, the signal is matched filtered to maximize the Signal-to-Noise Ratio (SNR). Another important property of matched filtering is it minimizes the Inter-Symbol Interference (ISI). Then the sampling time is determined and the signal is downsampled. The frequency offset estimation is the most challenging estimation block. There are some criterions to be considered for good estimation and correction and also modulation type is an important factor.

This study focuses on Nyquist pulse shaped quadrature amplitude modulation (QAM) signals and proposes blind synchronization and detection solutions to these kinds of signals. It is assumed that there is only one signal in the spectrum observed and it is Nyquist pulse shaped.

1.1. Organization of Thesis

There are six chapters in this thesis. In Chapter 2 the bandwidth and carrier frequency algorithms and their simulation results are discussed. Chapter 3 describes one of the most important parameters in blind demodulation which is the symbol rate of the signal. In this chapter the proposed algorithm's performance is evaluated and compared to the results in the literature. In Chapter 4, pulse shape and optimum sampling time estimations are discussed. Modulation identification, frequency and phase offset estimation and correction algorithms are introduced in Chapter 5 of this study. Chapter 6

includes the conclusion part of this thesis and discusses the performance of the proposed algorithms.

CHAPTER 2

BANDWIDTH AND CARRIER FREQUENCY ESTIMATION

2.1. Introduction

Bandwidth is the occupied space in the frequency spectrum. The information is transmitted over this whole bandwidth. It is desirable to transmit large data sets in small amount of bandwidths since bandwidth is limited. In order to achieve this goal, larger modulation orders are used.

Carrier frequency is the frequency used to transmit the information. The signal is centered at this frequency and has a variance of half of the bandwidth to the right and to the left of the carrier. The scope of this chapter will be on estimating these two features which form the first two steps of a blind receiver. Especially bandwidth estimation is important since symbol rate is related to the bandwidth.

This chapter is organized as follows. In Section 2.2, bandwidth definitions, bandwidth estimation and challenges are discussed and simulation results are provided. Carrier Frequency estimation, challenges and simulation results are provided in Section 2.3.

2.2. Bandwidth Estimation

The bandwidth is a crucial factor needs to be considered when designing a system. Every system has different bandwidth depending on their usage. The available spectrum is limited, and there are some regulations to use this spectrum which are

employed by Federal Communications Commission (FCC). Within these regulations there are some bandwidth limitations for designing the system.

2.2.1. Literature Overview and Challenges

The bandwidth estimation is the first step in blind demodulation. This is a required parameter for the estimation of the carrier frequency, and also this parameter creates some room for the estimation of symbol rate in Nyquist pulse shaped signals. In this kind of signals, the bandwidth is related to the symbol rate and the roll-off factor which are going to be discussed in following chapters. It is also important for the carrier frequency estimation since the bandwidth is divided equally over the carrier frequency.

There are different types of bandwidth: absolute bandwidth, null-to-null bandwidth, effective bandwidth, $3\ dB$ bandwidth and $10\ dB$ bandwidth. Null-to-null bandwidth is the width of the main lobe of the signal (in this work null-to-null bandwidth is estimated). This bandwidth type is not suitable for all modulation types since they lack of generating side lobes. Absolute bandwidth can be interpreted as the width of the spectrum between two frequencies where the rest of the spectrum is zero. $3\ dB$ bandwidth is measured when the signal drops $3\ dB$ below its maximum power, and $10\ dB$ bandwidth is measured in the same way. $3\ dB$ bandwidth is a good measure for Nyquist pulse shaped signals since it is equal to the symbol rate in the perfect case. $3\ dB$ bandwidth is also referred as half-power bandwidth.

2.2.2. Method Proposed

For the estimation of (null-to-null) bandwidth, a simple energy detector algorithm is used. A noise floor is defined and according to this noise floor, the start and end frequencies are determined, where the width of this lobe gives the bandwidth. The signal

is passed through a random channel, which is the combination of additive white Gaussian noise (AWGN) and a slightly dispersive channel, and each symbol has different amount of energy. Because of these two reasons, the spectrum of the signal will not be smooth, which will cause a wrong estimation of bandwidth. The received signal spectrum is passed through a window to remove the fluctuations due to the channel. The main purpose for windowing will be discussed later.

The next step of the method is determining the noise floor. A baseline is always necessary for energy based approaches (energy detector). While determining the noise floor, the total energy of the signal is calculated, and using the total energy value, the noise floor is calculated and assumed to be 10% of the total energy. Basically, the mean of these samples form the reference point (power threshold) for bandwidth estimation. But in some cases, due to the high fluctuations in the channel this level may lead to false results (during some frequency bands this threshold might be less than the noise). In order to prevent these challenges, this level is increased to a higher value and the first sample higher than this level is considered to be the starting frequency of the information. The ending frequency is determined in the same way, but in an opposite manner. The distance between these two estimated frequency bins represents the (null-to-null) bandwidth of the signal.

This approach is valid for slightly dispersive channels. In high dispersive channels, due to the high fluctuations in the spectrum, this algorithm may not give correct results and may mislead the estimations of other related parameters (such as the carrier frequency), which will fail the perfect demodulation process.

An important feature of this energy based method is that it is not computationally complex, which is a desirable property in real time synchronization and demodulation. The method is modulation independent and the performance of the algorithm is proven to be considerable throughout the computer simulations.

2.2.3. Simulation Results

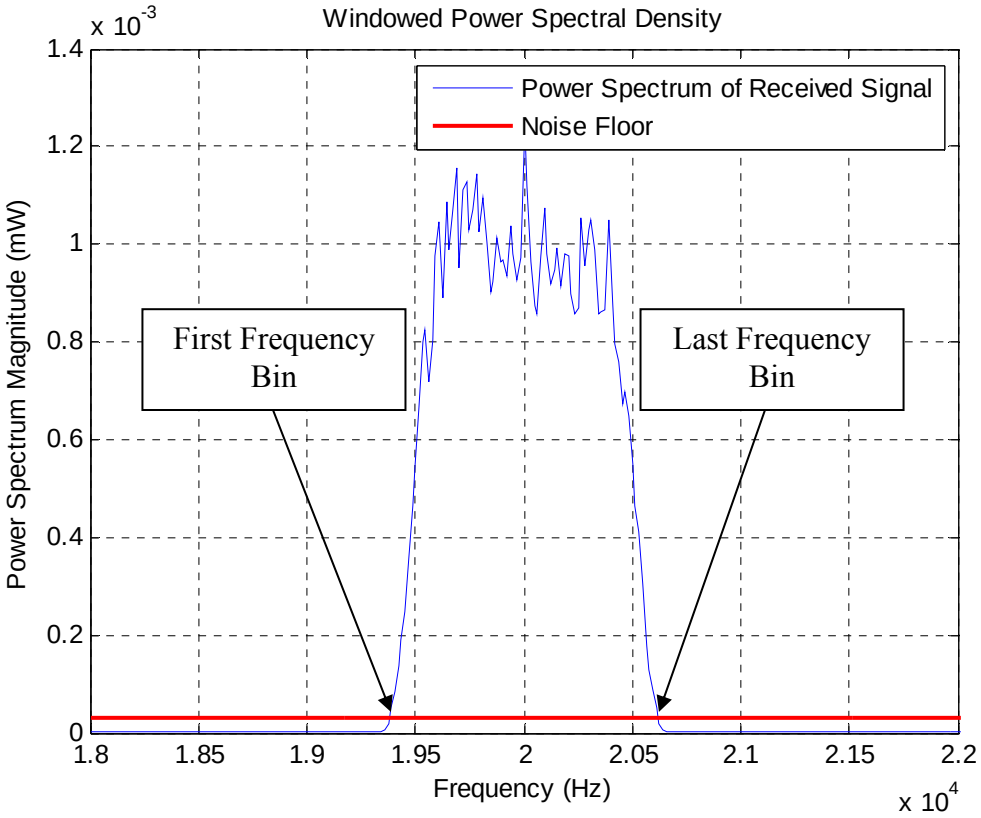

Figure 2: Bandwidth Estimation

The signals are first generated in the baseband and then they are shifted to some frequency, suppose $20\ kHz$. The received signal is windowed and the noise floor is determined. As the proposed method suggests, any frequency bin having a magnitude larger than the noise floor value lies inside the signal bandwidth. So, in order to calculate the bandwidth, the first frequency bin having larger magnitude than the noise threshold

and the last frequency bin having larger magnitude is considered. The width of these two frequency bins represents the bandwidth of the signal.

The simulations are performed with symbol rate of 1 $kSps$ (kHz), with a roll-off factor $\alpha = 0.35$, oversampling rate $N = 16$, and SNR of $15dB$ in a single tap AWGN channel. The theoretical estimation of the absolute bandwidth is $1.35\ kHz$ and the modulation type used is 4QAM.

In Figure 2, the noise floor and the power spectral density (PSD) of the signal with the parameters above are illustrated.

2.3. Carrier Frequency Estimation

Carrier frequency is the frequency component where the information is carrier on with a bandwidth of W. The system used in the transmitter determines the carrier frequency and it is also regulated by FCC. If the transmitter is operating in the ISM band it should be in the specified frequency range. In the literature there is not much published on carrier frequency estimation.

2.3.1. Literature Overview and Challenges

The estimation of carrier frequency should be done as close enough to minimize the frequency offset in the system. If the signal is assumed to spread equally over the carrier frequency the middle point of the band should give the carrier frequency.

2.3.2. Method Proposed

Carrier frequency estimation is another important feature in blind demodulation applications. The signal is processed in the baseband and since all the signals taken into consideration in this study are in the IF band, they need to be downshifted to baseband. Throughout the simulations, depending on the significant success of the technique used,

the carrier frequency estimation algorithm is based on estimating the middle point of the signal. With its low computational complexity and proven efficiency, this basic algorithm is used for the estimation of the carrier frequency. As stated above, this estimation will not be perfect due to the random nature of the channel and the remaining part will be corrected in the following steps and will be discussed in the Modulation Identification, Frequency and Phase Offset Estimation and Correction chapter. Let $c(i) = a(i) + jb(i)$ denote the transmitted symbol sequence and consider that the symbols are independently and identically distributed. The transmitted symbol sequence is given by,

$$s[n] = \sum_i c[i]h[n-i] \qquad (2.1)$$

where h, represents the pulse shaping filter used at the transmitter. The received signal model is given by,

$$r[n] = \sum_i c[i]h[n - iT_s] + \omega[n] \qquad (2.2)$$

In the above equation r, T_s and ω represents the received symbol sequence, sampling time and the AWGN due to the channel respectively. After the carrier frequency estimation, using the estimated value from this step the signal is downshifted to the baseband. And the signal model in baseband is given by,

$$r_{baseband}[n] = r[n]e^{j2\pi f_{est} nTs} \qquad (2.3)$$

where f_{est} represents the estimated carrier frequency. If $f_c \neq f_{est}$, when the signal is downshifted to baseband, because of the wrong carrier synchronization there will be a frequency offset Δf, where $\Delta f = f_c - f_{est}$, which will be discussed and corrected in Chapter 5.

2.3.3. Simulation Results

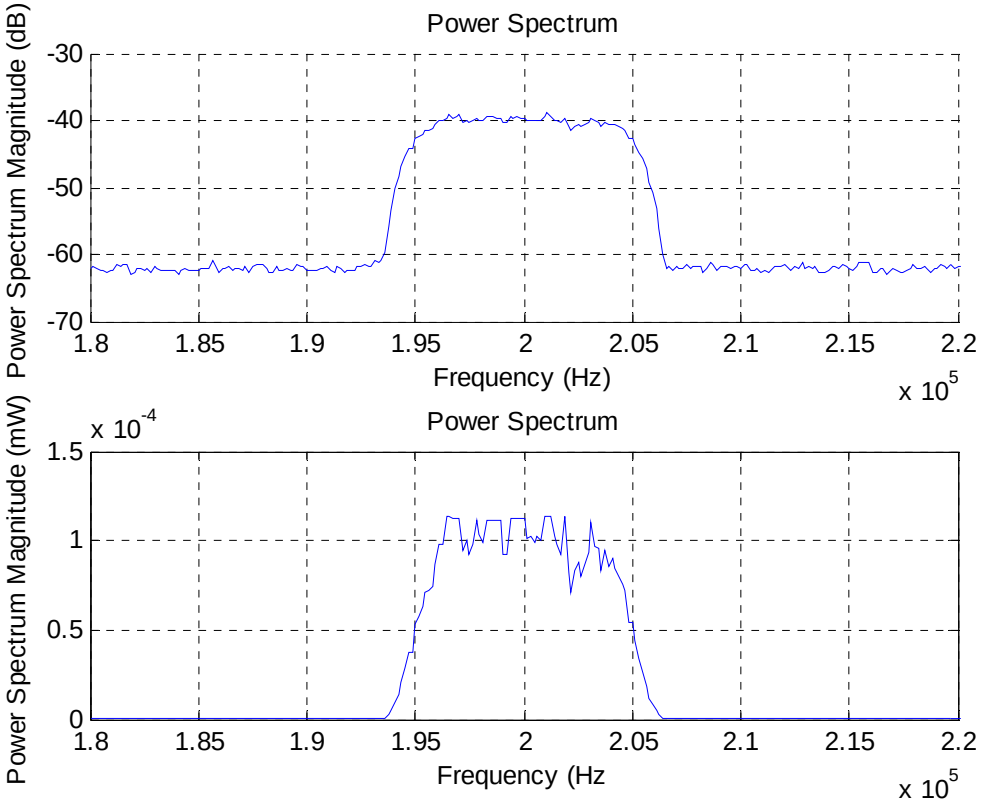

Figure 3: Carrier Frequency Representation

The carrier frequency estimation is proposed to shift the signal to the baseband. This estimation should be as accurate as possible to avoid high frequency offsets. The method suggests that the carrier frequency is in the middle of the signal. With a simple math this can be done; the mean of the start frequency and end frequency.

The signal considered has a carrier frequency of $200\ kHz$ and has the same parameters as the bandwidth estimation chapter (Symbol Rate = $10\ kSps$, Root Raised Cosine Filter with $\alpha = 0.35, N = 16, SNR = 15dB$). In an AWGN channel, the performance of the proposed method is close to perfect.

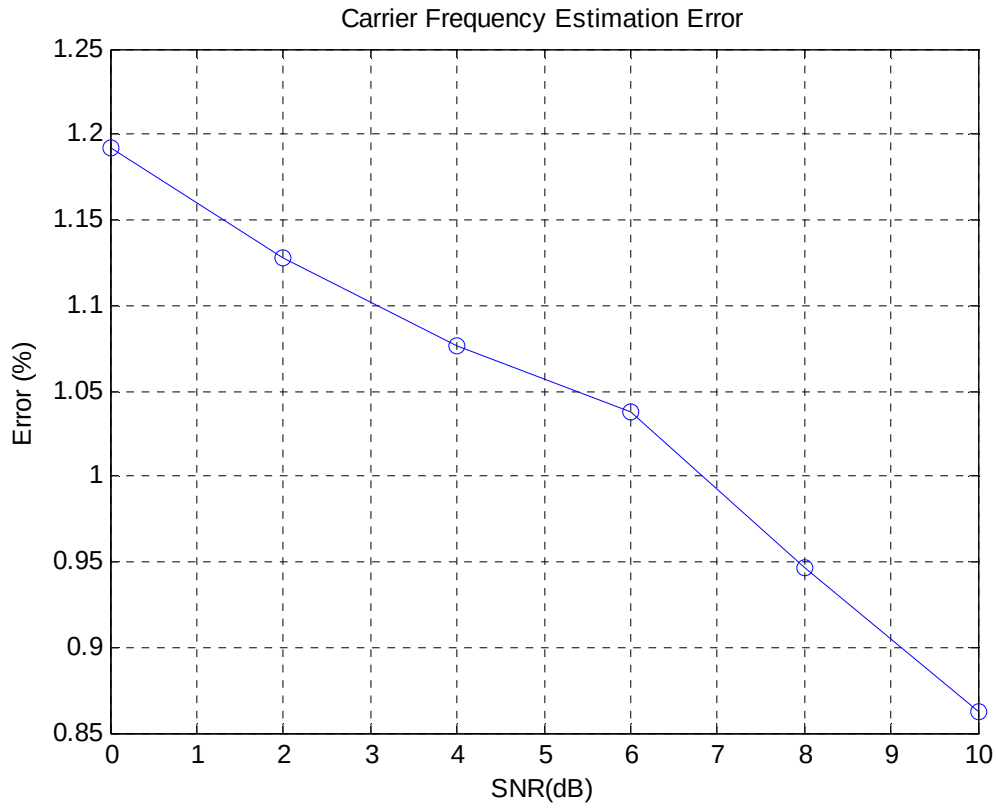

Figure 4: Carrier Frequency Estimation Error

In Figure 3, the power spectrum can be seen in both logarithmic and linear scale. It is suggested that the carrier frequency is in the middle of the band.

$$e = \frac{|f_{est} - f_c|}{W} \times 100 \qquad (2.4)$$

where f_{est}, f_c and W represent the estimated carrier frequency, actual carrier frequency and the bandwidth respectively. It is not surprising to see that estimation error decreases when SNR is increased. The simulation is performed with 4QAM and a symbol rate of 10 $kSps$ at 200 kHz.

CHAPTER 3

SYMBOL RATE ESTIMATION

3.1. Introduction

Symbol rate is often referred as baud rate or data rate meaning that how many symbols sent per second. It is also related to the bandwidth, i.e. as symbol rate increases bandwidth also increases and vice versa. The estimation of symbol rate is a very crucial item in blind receivers since most of the parameters to be estimated depend on the symbol rate.

Symbol rate estimation is performed in three steps: coarse, fine and refinement steps. In the coarse estimation step a rough estimation of symbol rate is performed and in the fine estimation step, using the value from the previous step a better estimation is performed. Then the remaining residual errors are corrected by using suitable timing recovery algorithms [3, 4, and 5]. A block diagram of three step symbol rate estimation is provided in Figure 5.

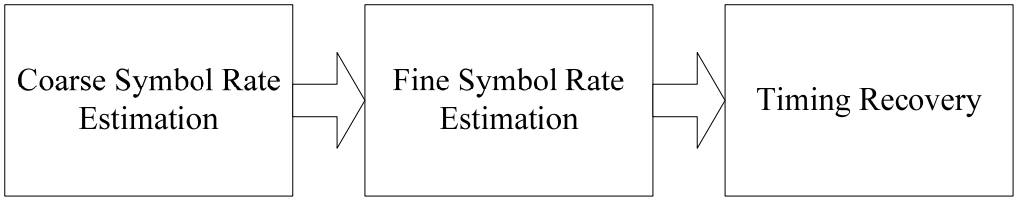

Figure 5: Block Diagram of Symbol Rate Estimation – Coarse Estimation, Fine Estimation and Timing Recovery

This chapter is organized as follows. In Section 3.2 the challenges in the symbol rate estimation will be discussed and the estimation algorithms in the literature are introduced. Section 3.3 introduces the proposed method for the symbol rate estimation and in Section 3.4 numerical and simulation results are discussed.

3.2. Literature Overview and Challenges

All of the digitally modulated signals require the knowledge of symbol rate for demodulation. It is one of the most crucial parameters for demodulation. Up until the estimation of symbol rate, there is no other parameter is known. There are many papers published in this area using different methods such as Wavelet Transform [6], Inverse Fourier Transform (IFT) [7, 8], Filter Bank [9], Cyclic Correlation Based [10,11 and 12] and Cyclostationarity [13, 14 and 15]. Some of these algorithms are only coarse estimation algorithms and some of them are fine estimation algorithms. There is no such algorithm in the literature that performs fully blind symbol rate estimation. The coarse estimation algorithms do not perform well; on the other hand, fine estimation algorithms require the knowledge of the symbol rate.

The wavelet transform based algorithm is first proposed by K.C.Ho [6] et al. and this algorithm was based on locating the phase changes between the symbols. The symbol rate was assumed to be the distance between two located phase changes. In wavelet transform based approaches, it is very important to choose the most proper scale value. In this work, the authors have chosen the scale to be a very small number. The first algorithm on this topic was using only one scale for wavelet to estimate the symbol rate, then the algorithm was improved and several scales for wavelet were used to estimate the symbol rate. The use of several scales gave more information about the signal, since

each scale will produce a different output of the signal. These scales were added together and then the resulting signal is inspected for the estimation of the symbol rate. The previous work intended to work with M-ary phase shift keying (MPSK) signals, and then Zan-Ji et al. [16] improved this work to estimate the symbol rate for QAM, pulse amplitude modulation (PAM) and frequency shift keying (FSK) signals as well. A high SNR, high oversampling rate and large bandwidth is required to have a better estimate for the symbol rate for this algorithm.

Another algorithm for the estimation of the symbol rate is the IFT based algorithm which was proposed by Koudelka et al. [7] and this algorithm was based on converting the received time signal into the frequency domain. Then using IFT operation, it calculates the magnitude of the filter. With an assumption of pulse shaping filter used is a Nyquist filter, observing the samples between the peak and the first zero-crossing the symbol rate can be estimated. But due to the high channel effects, this estimation is inaccurate in multipath environments. A proposed method is to resample the signal and then observing the samples between the peak and the first-zero crossing, which will give a better estimation of the symbol rate. This algorithm works well in non-fading channels and with both integer and non-integer valued oversampling rates.

One other method used is based on filter banks which is much more computationally complex compared to other algorithms. The received signal is passed through a bank of low pass filters. Then the output is inputted to a nonlinear unit. The output of the nonlinear unit has peaks at several locations and the algorithm chooses the most possible one by majority voting and assigns it as the symbol rate [9].

Cyclic correlation based algorithms estimate the symbol rate by generating spectral lines. The spectral line generation process is proposed by Gardner [13, 17]. The spectral line generation is done by simply taking the fast Fourier transform (FFT) of the square of the signal. This process extracts the hidden periodic information of the signals. By inspecting the output of this process, it can clearly be seen that at low excess bandwidth conditions the peak cannot be seen clearly. To increase the accuracy of this estimation at low excess bandwidth conditions, Mazet and Loubaton [10] proposed an algorithm to overcome this problem. This algorithm was based on a weighting matrix proposed by Dandawate and Giannakis [18]. This process is computationally complex but a very efficient algorithm. Another method to overcome this low excess bandwidth condition was proposed by Reichert [11] et al. and was a very simple algorithm. Its basics were founded on removing the shape of the output of the cyclic correlation function by windowing and subtracting it from itself. By doing this, the peak is very easy to detect.

One of the most accurate estimation processes used to estimate the symbol rate is cyclostationarity approach. Every digitally modulated signal has some periodic parameters such as symbol rate, modulation type, chip rate and carrier frequency and cyclostationary analysis may be applied to these kinds of signals. Gardner [13, 14, 15 and 17] named these kind of signals cyclostationary signals and proposed a method to determine these parameters. This method is a computationally complex method if the data is too large, but it gives very accurate estimates. The idea lying behind this method is extracting the periodic information in the second moment of the signal. Equations 3.1 and 3.2 show the signal model of cyclostationarity analysis. In this algorithm, first the correlation of the signal with the conjugate of itself in different lags is calculated. Then

this signal is represented with Fourier coefficients. Basically, a Fourier transform is taken at cycle frequencies α. When α is equal to the symbol rate, a spectral line is observed. Some modulation types have carrier frequency related spectral lines but some other do not have carrier frequency related spectral lines. Since the focus is on symbol rate estimation, the carrier frequency estimation using cyclostationarity analysis is not considered right now. The output of the FFT operation is called cyclic correlation function. This function consist elements for α and τ values, where α and τ represent the cyclic shift and lag respectively. Then the spectral correlation density (SCD) function is calculated by taking the FFT of the cyclic correlation function with respect to lag τ. The SCD has the elements which are related to cyclic shift α, and the frequency f. To obtain the symbol rate using cyclostationary analysis, the span of α must contain the whole band, which makes it computationally complex. There are some other algorithms which are computationally less complex such as Frequency Smoothing Method (FSM), FFT Accumulation Method (FAM) and Strip Spectral Method (SSM), which are not discussed in this chapter [19, 20].

$$\widehat{R_x^{\alpha}(\tau)} \triangleq \frac{1}{T_0} \int_{-\infty}^{T_0} \widehat{R_x}(t,\tau)\, e^{-j2\pi\alpha t} dt \qquad (3.1)$$

where,

$$\widehat{R_x}(t,\tau) \triangleq \lim_{N\to\infty} \frac{1}{2N+1} \sum_{n=-N}^{N} x\left(t + nT_0 + \frac{\tau}{2}\right) x^*\left(t + nT_0 - \frac{\tau}{2}\right) \qquad (3.2)$$

Equation 3.2 is referred as the cyclic autocorrelation function where α is the cycle frequency, T_0 is the period, τ is the time lag and * represents the complex conjugate.

3.3. Method Proposed

The proposed method consists of two parts; coarse estimation and fine estimation [21]. This section describes both methods in detail and a block diagram can be found in Figure 6.

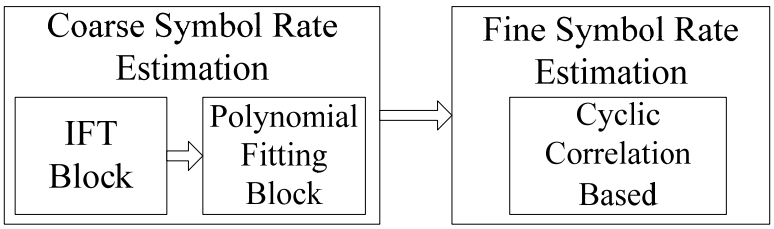

Figure 6: Block Diagram of Proposed Symbol Rate Estimation Method

The coarse estimation step of the proposed method depends on IFT based algorithm [7]. Let $c(i) = a(i) + jb(i)$ denote the transmitted symbol sequence and consider that the symbols are independently and identically distributed and $j = \sqrt{-1}$. Considering the zero-mean AWGN to be $\omega(t)$, the received signal can be written as,

$$r(t) = e^{(-j2\pi\Delta f t + j\theta)} \sum_i c(i)h(t - iT - \tau) + \omega(t) \qquad (3.3)$$

where τ, Δf and θ represent the time shift, frequency offset and phase offset respectively and h is the impulse response of the pulse shaping filter, and assumed to be a root raised cosine filter with a roll-off factor α, where $0 \leq \alpha \leq 1$.

All the procedures are same as this method until the resampling step. The power spectrum is computed by averaging the related periodograms [22, 23] and the IFT of the power spectrum is taken. The output of these processes is the raised cosine pulse. If there is a raised cosine pulse, number of samples between the peak and the first horizontal axis crossing gives the oversampling rate, which is the case here. Also, the first horizontal axis crossing will occur at the sampling time which is the multiplication of the symbol

rate and the oversampling rate. Now, a rough estimation of the symbol rate is obtained. In real life, oversampling rate is not an integer all the times. It is totally related to the sampling rate of the system. Considering the channel effects and the issue mentioned, there will be no sample at the first horizontal axis crossing. A method is proposed by Koudelka et al. [7]. According to this method, the signal is resampled and the resolution is increased.

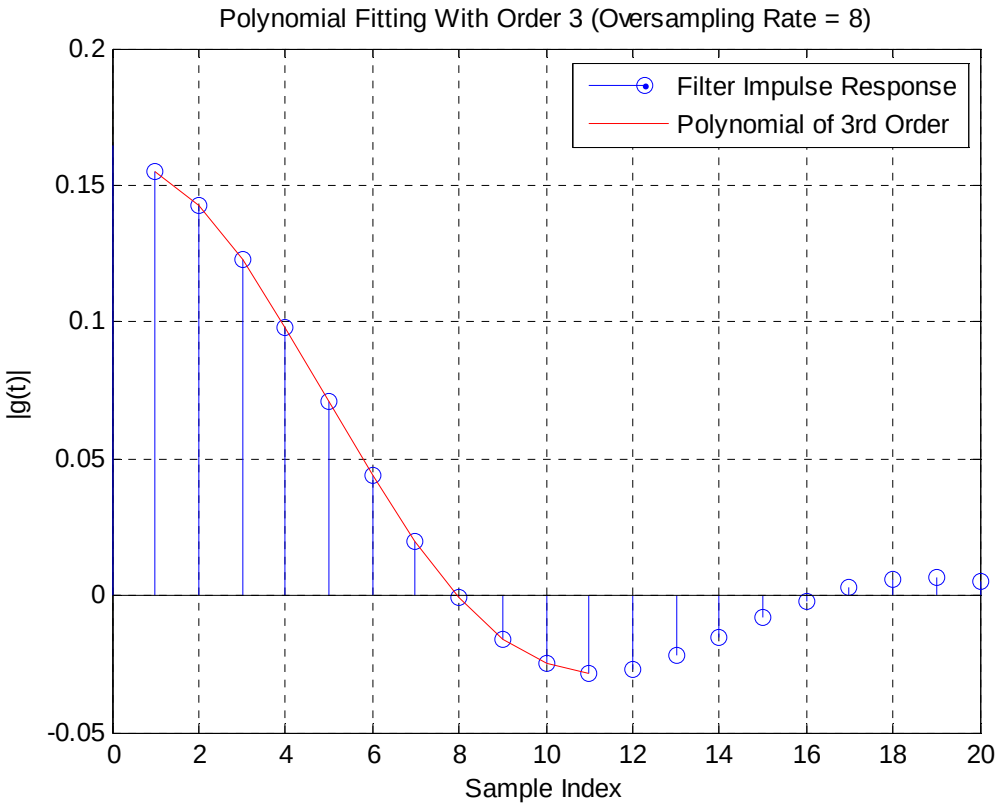

Figure 7: Representation of Polynomial Fitting

Another way of finding the number of samples between the peak and the first horizontal axis crossing is to have a polynomial fitted to these samples. By fitting a polynomial of third order between the peak and the next absolute peak after the zero crossing, this problem can be solved. The order of polynomial is chosen to be three after numerous simulations with different roll-off factors. It is the least order having the best

estimation performance with different roll-off factors. This method is the rough estimation step of the symbol rate. The estimation performance of this step is very important since it is going to be used in the fine estimation stage which is a cyclic correlation based algorithm. Figure 7 denotes an example for polynomial fitting for a raised cosine pulse with an oversampling rate of 8. In this example there is no channel considered and there is a sample on the horizontal axis at the 8th index, which is expected. But when the channel effects are considered, there will be no sample on the horizontal axis.

The second stage of the algorithm is the fine estimation step. It is a cyclic correlation based algorithm. This step uses the periodic features of the signal to generate spectral lines. Consider the signal model in equation 3.3. The signal is squared and FFT of the signal is taken. The squared received signal is given by,

$$y(t) = r^2(t) = \sum_i d(i)q(t - nT - \tau) + \omega^2(t) \qquad (3.4)$$

where $d(i) = c^2(i)$ and $q(n) = h^2(n)$.

The PSD of $y(t)$ is given by,

$$S_y(f) = \frac{1}{T}|Q(f)|^2 \sum_n S_d\left(f - \frac{n}{T}\right) \qquad (3.5)$$

where $Q(f)$ is the Fourier transform of $q(t)$.

The spectral lines are generated by using the method proposed by Gardner [13, 17]. The proposed method generates more than one spectral line which are at k/T, $k \epsilon Z$. There are some challenges for picking the symbol rate spectral line in low excess bandwidth cases. Excess bandwidth is related to the roll-off factor of the filter used at the transmitter. It is also called as the bandwidth larger than the Nyquist bandwidth. If the

roll-off factor used at the transmitter is low, i.e. excess bandwidth is low; the spectral line generated will not be seen clearly. This can be easily seen in Figure 8. It is obvious that the spectral line disappeared inside the bandwidth of the signal when the roll-off factor is low. But when roll-off factor increases, the spectral line is clearer.

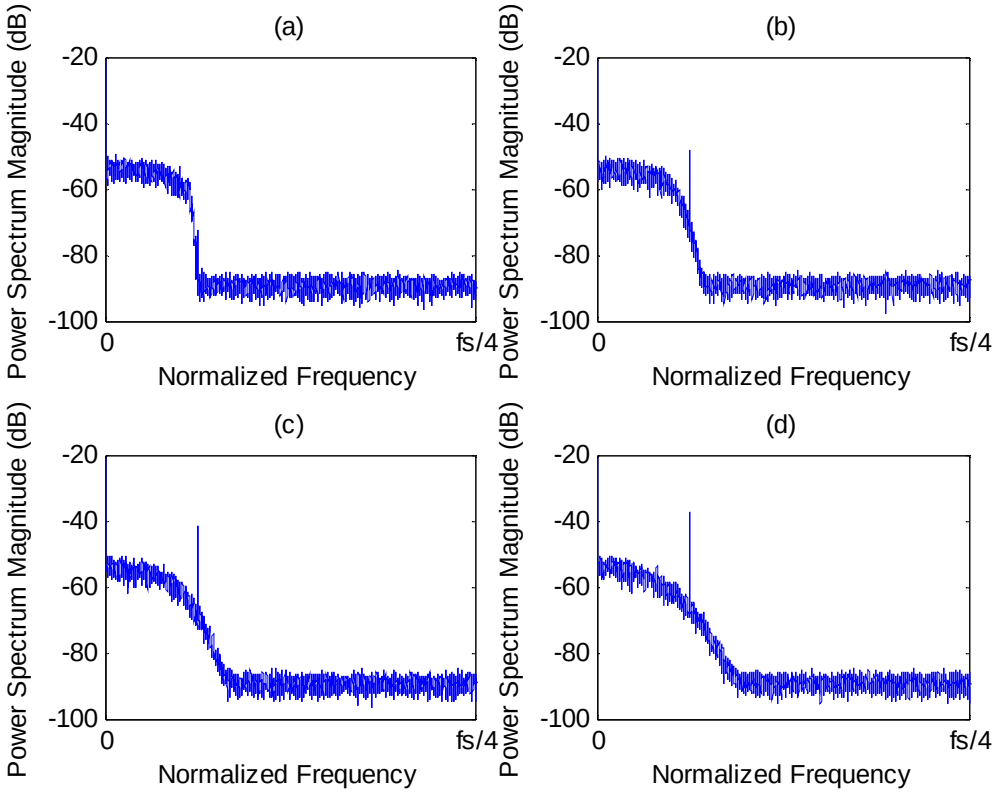

Figure 8: Effect of Excess Bandwidth on Spectral Line Generation for Cyclic Correlation Based Algorithms. (a) 0% Excess Bandwidth (b) 30% Excess Bandwidth (c) 60% Excess Bandwidth (d) 100% Excess Bandwidth

There are some methods proposed to overcome this problem. One of these algorithms is based on flattening the spectrum of the signal by using singular value decomposition [10]. In the search range, the inverse discrete Fourier transform of the estimator matrix is calculated which brings a huge computational complexity which is not

desirable. Another method proposed to overcome this problem operates in spectral domain [11]. The received spectrum is smoothened and is subtracted from itself. By employing this method the shape of the spectrum is removed. Since the samples are averaged within a window, the spectral line is not affected from this subtraction operation. In this approach, after this subtraction operation, the spectral line due to the symbol rate becomes clearer to see.

The proposed fine estimation step is based on creating a search region for cyclic correlation based algorithms to overcome the low excess bandwidth problem. The search region is determined by using the estimation in the coarse estimation step. By using this kind of approach, the computational complexity is reduced compared to the algorithm proposed by Mazet et al. The size of the search region is also an important factor. If the search region is too small, the system becomes more error proneness as it can choose a spectral line generated due to the noise in the channel. On the other hand, if the search region is large, the computational complexity is higher than the normal case.

The oversampling rate is estimated jointly with the symbol rate. Oversampling rate is the ratio of sampling rate to the symbol rate and an important factor for pulse shape estimation, optimum sampling instant estimation and downsampling. A mistake in estimating the oversampling rate causes wrong results.

3.4. Simulation Results

The simulations are done using a single carrier 16QAM signal with symbol rate of $8.192\ MSps\ (MHz)$, roll-off factor $\alpha = 0.35$, oversampling rate $N = 19.53125$, and SNR values between $-5\ dB$ and $5\ dB$ with $2\ dB$ increments. Simulation results show

that, the proposed method performs much better than the IFT based method [7] both in complexity and performance aspects.

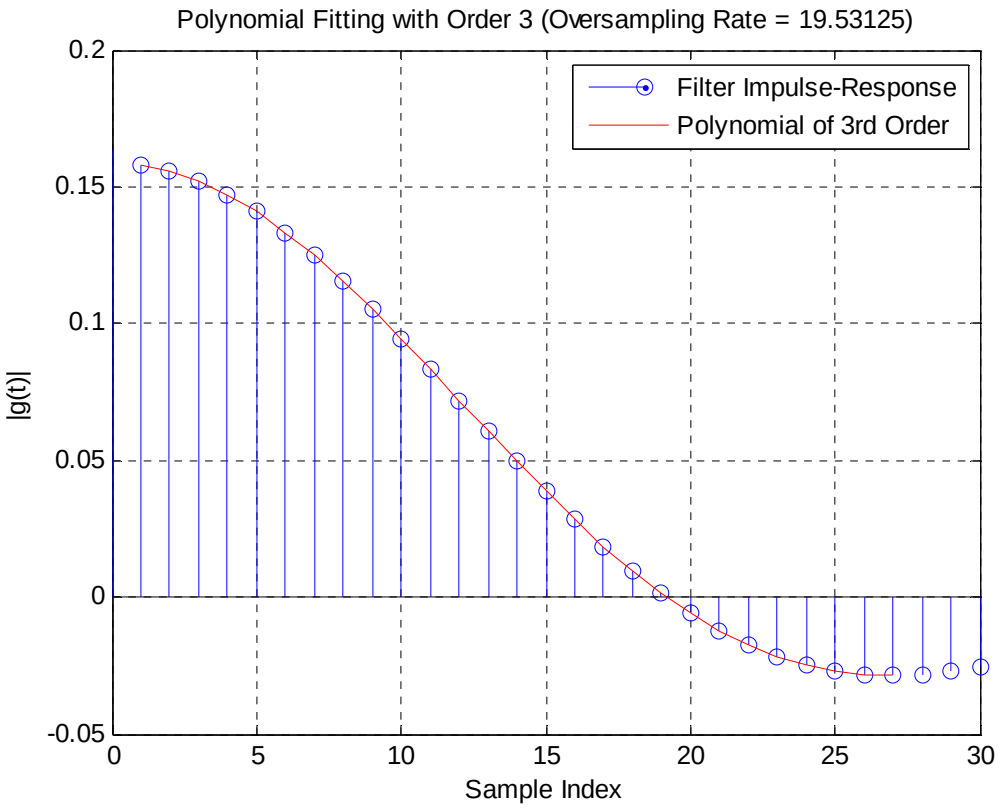

Figure 9: Coarse Estimation Part of Proposed Method. (a 3rd Order Polynomial is fitted)

The results are evaluated based on the Root Mean Square Error (RMSE) and the success rate, where a success is considered to be a %3 deviation from the true symbol rate. The proposed method is compared to two different versions of IFT based method [7]; one with a resampling rate of 4, the other with 64.

In Figure 9, polynomial fitting block of the proposed coarse estimation is illustrated. The zero-crossing occurs after the 19th sample and a more precise estimation of symbol rate is achieved.

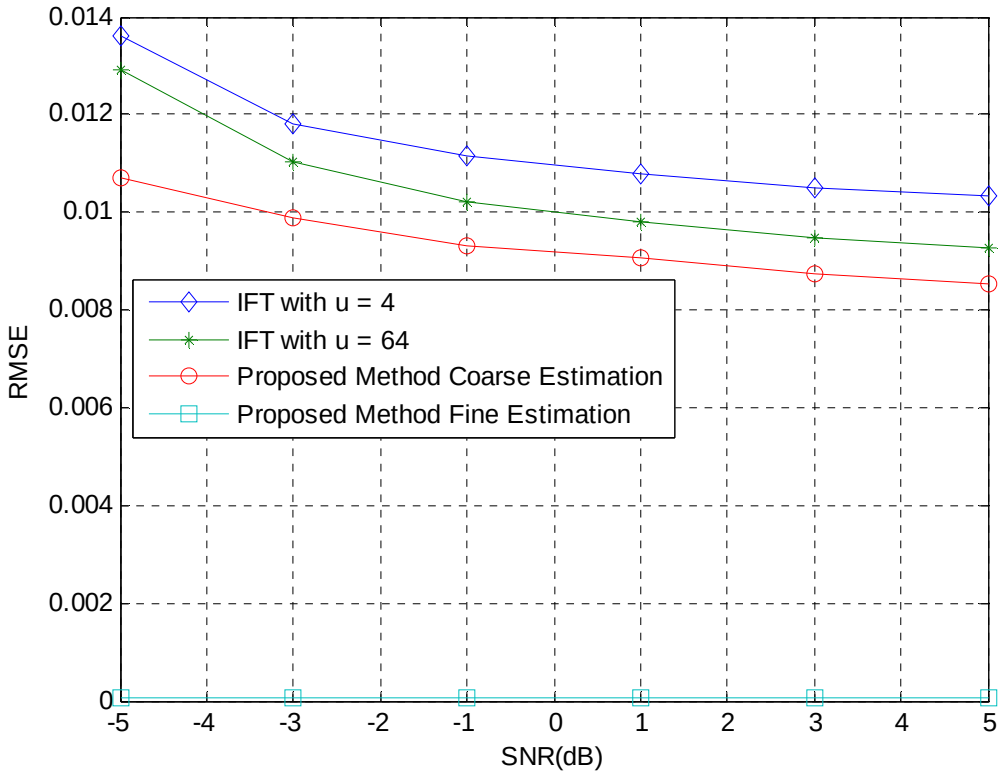

Figure 10: RMSE Performance of Proposed Method Compared to [7]

Figure 10 shows the RMSE of the proposed methods performance at the coarse and fine estimation steps as well as the IFT based methods performance at two different resampling rates. When the resampling rate is small, the complexity of the algorithm is less but the performance is worse since the resolution is low. When the resampling rate is increased, the performance gets better as well as the complexity increases. With a third order polynomial fitted between the peak and the next absolute maximum of the generated Nyquist pulse the performance of the method is better in both RMSE and complexity aspects.

In Figure 11, evaluation of success rate is shown. The coarse estimation step of the proposed method increases the success of [7] around 1% and when the fine estimation

step is performed, the success rate is increased to 100%. It can be seen that, regardless of the SNR value, the performance of the cyclic correlation based algorithm is significant.

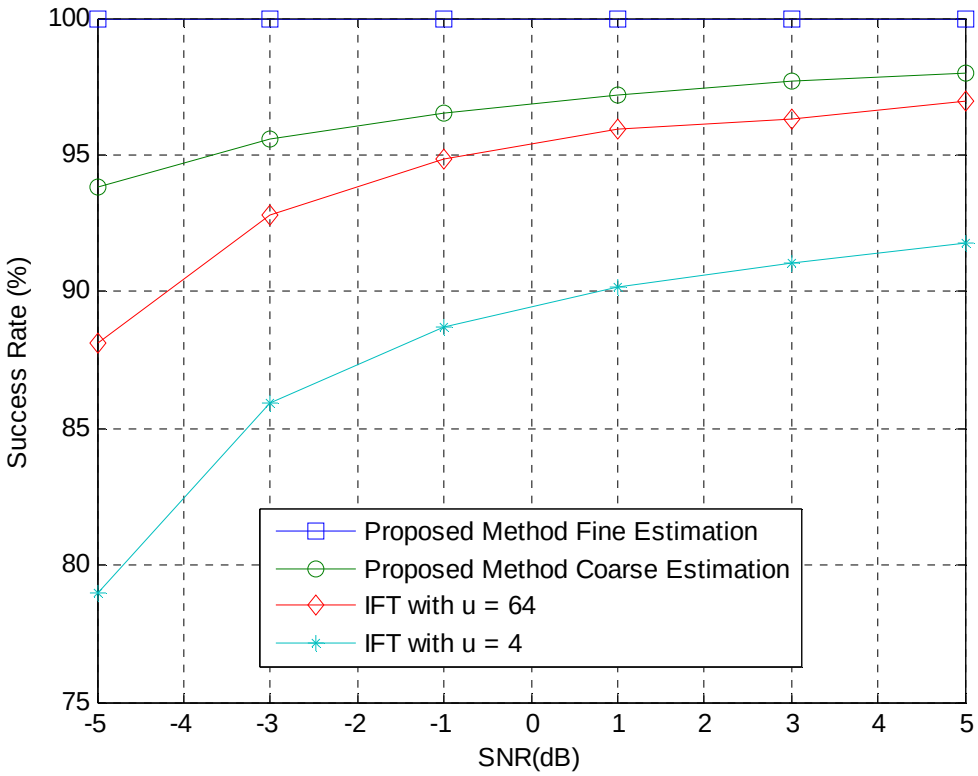

Figure 11: Success Rate of Proposed Method Compared to [7]

CHAPTER 4

PULSE SHAPE AND OPTIMAL SAMPLING PHASE ESTIMATION

4.1. Introduction

The pulse shaping filter effects the bandwidth of the signal and it is related to the inter-symbol interference (ISI). The roll-off factor of the filter is directly related to the bandwidth of the signal where as the filter type affects the ISI. If the filter used is a Nyquist filter, such as a raised cosine filter (or combination of two root raised cosine filters in the transmitter and receiver, i.e. matched filtering), there will be no ISI introduced to the system.

Pulse shape estimation includes the roll-off factor estimation for the matched filtering process. In blind receivers, the roll-off factor is a crucial parameter to be estimated for perfect demodulation. If the roll-off factor of the transmit filter and the matched filter (if required) are the same, it means that the system is performing in its best performance level. Also, roll-off factor is a measure for the excess bandwidth. Excess bandwidth can be named as the bandwidth larger than the Nyquist criterion.

Optimum sampling instant is the instant where the signal is sampled. If the filter used at the transmitter is a Nyquist filter, at this instant the signal has the highest energy. In order to perfectly demodulate the signal, the signal should be downsampled at the optimum sampling instant, otherwise the system will introduce ISI.

This chapter is organized as follows. In Section 4.2, the Nyquist criterion is discussed. Section 4.3 focuses on the pulse shape estimation and discusses the challenges in roll-off factor estimation. Optimum sampling instant is explained in detail in Section 4.4. Simulation results are discussed in Section 4.5

4.2. Nyquist Criterion

A signal is considered to be bandlimited if there is no energy stored at frequencies greater than some bandwidth W. According to Nyquist sampling theorem an analog signal can be reconstructed from the samples taken if it is bandlimited.

$$X(\mathrm{f}) = \int_{-\infty}^{+\infty} \mathrm{x(t)e^{-j2\pi ft}dt} \qquad (4.1)$$

X(f) represents the Fourier transform of a continuous signal $x(t)$. According to the Nyquist criterion, in order to have the signal bandlimited, $X(f)$ should be 0 for all$|f| > W$.

Nyquist sampling theorem states that, the sampling rate f_s, should be larger than twice the bandwidth, i.e. $2W$, where $2W$ is the Nyquist rate and $f_s/2$ is the Nyquist frequency.

Suppose a received analog signal $r(t)$. Every T second a measure is taken. In discrete domain, this signal is represented as $r(nT_s)$, where T_s is the sampling time and $T_s = 1/f_s$. These samples are taken from the original analog signal. Then, all of the samples are multiplied by a $sinc$ function and interpolated. $sinc$ functions do not create any interference to other samples, since they are 0 at sampling instants except the original instant. If the signal is bandlimited, the reconstruction will end up the same as the original signal [24, 25 and 26].

4.3. Pulse Shape Estimation

Pulse shape is determined by the filter used in transmitter. System requirements define the pulse shape to be used in the transmitter. If ISI is an important criterion, filters obeying Nyquist criterion may be used, if other criterions are important Gaussian or Chebyshev type of filters might be preferred.

4.3.1. Literature Overview and Challenges

The pulse shape estimation is not studied widely in the literature and left as a big problem. In [8], the roll-off factor of the filter is estimated by observing the main peak and the second peak. It is stated that, the amplitude fluctuations are relative to the roll-off factor of the filter where roll-off factor lies between 0 and 1.

In this work, the assumed filter used in transmitter is a Nyquist filter such as Raised Cosine or Root Raised Cosine Filter. Raised cosine filtering maintains zero-ISI when sampled at the perfect sampling instant and maximizes the SNR when matched filtering operation is performed (if required). Raised cosine filtering creates 0 impulse-response at the correct sampling instants to other symbols, which cancels the ISI effect. The transfer function of raised cosine filter is defined as;

$$H(f) = \begin{cases} T, & |f| \leq \frac{1-\alpha}{2T} \\ \frac{T}{2}\left[1 + cos\left(\frac{\pi T}{\alpha}\left[|f| - \frac{1-\alpha}{2T}\right]\right)\right], & \frac{1-\alpha}{2T} < |f| < \frac{1+\alpha}{2T} \\ 0, & otherwise \end{cases} \quad (4.2)$$

where α is the roll-off factor of the filter and lies in the interval [0,1]. Also α represents the excess bandwidth. For example, when α is 1, the excess bandwidth is %100. When α increases, the occupied bandwidth also increases and vice versa. The raised cosine filtering is chosen in many applications but when ISI is not an important criterion, it is

not desired. Gaussian and Chebyshev filters are the other mostly used filters. These filters do not guarantee zero-ISI but they are desirable in other aspects such as Gaussian filters are bandwidth effective and Chebyshev filters reduce the power leakage to adjacent channels. Raised cosine filtering also contains the root raised cosine filters. Root raised cosine filters are the same as raised cosine filters but unlike raised cosine filters, they are both in the transmitter and the receiver. The convolution of these root raised cosine filters forms a raised cosine filter. It is a result of the linearity of convolution operation. It is also important to note that root is taken in the frequency domain.

Figure 12 shows a raised cosine pulse with an oversampling rate of 16 and a roll-off factor α of 0.35. In this case, there is a zero-crossing at the 16^{th} instant, which occurs at the symbol period.

If the filter used at the transmitter is raised cosine filter, there is no need for matched filtering at the receiver. But if root raised cosine filter is used at the transmitter, to maintain Nyquist criterion requirements the received signal needs to be matched filtered with the same filter used at the transmitter. To match filter the signal with the same filter at the receiver, the oversampling rate and the roll-off factor needs to be known. The oversampling rate is calculated in the previous chapter during the symbol rate estimation. This estimation also needs to be accurate for match filtering. The only remaining unknown is the roll-off factor for matched filtering, which is discussed in this chapter.

At the receiver there is no knowledge about the roll-off factor. But since it is the third estimation step after the bandwidth and symbol rate estimations, depending on these

estimations there can be a rough idea about the α. The bandwidth of the signal is defined to be $(1 + \alpha)\ x\ f_{symbol}$, where f_{symbol} denote the symbol rate.

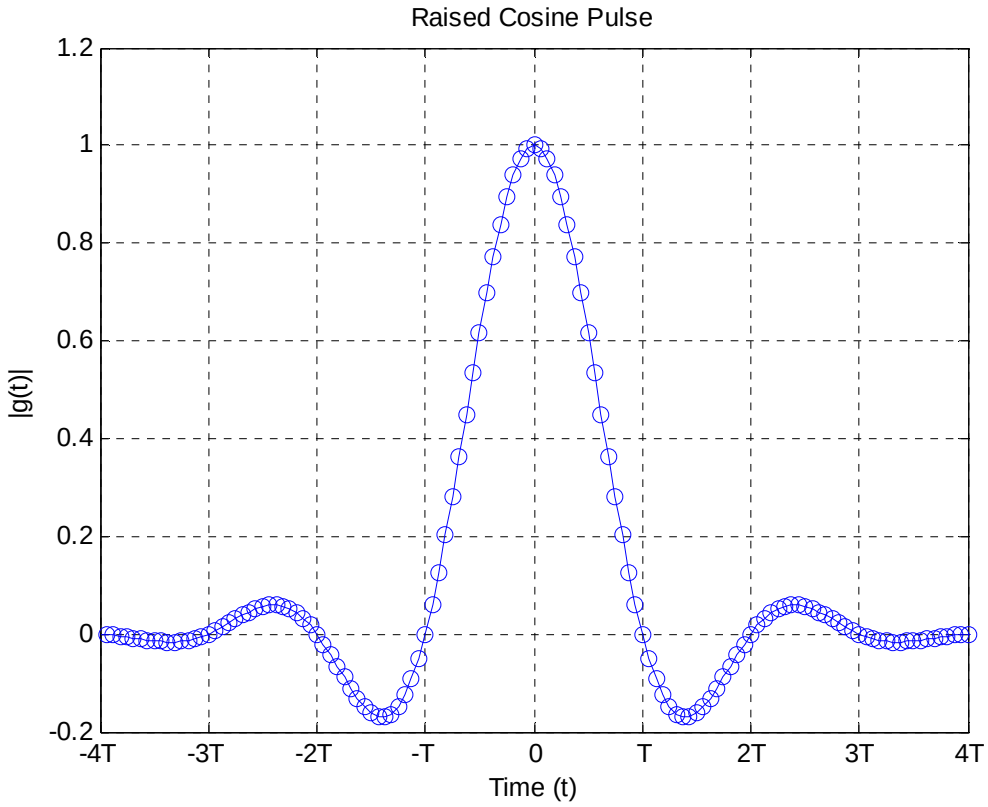

Figure 12: A Raised Cosine Pulse

4.3.2. Method Proposed

The method proposed is based on maximizing the SNR of the output of matched filtering process. The most important property of matched filters is they maximize the SNR. Another important feature of this process is they minimize the ISI. If the matched filtering process is done correctly, the signal will have the highest SNR. Also, when the signal is matched filtered with the correct roll-off factor, the eye diagram will look clearer when compared to others.

If the correct roll-off factor is chosen, the SNR of the convolution of the received signal with this match filter is maximized. This is a criterion for the perfect estimation of roll-off factor. The eye diagram is very clear when a matched filter used with the same parameters at the receiver. There are some pre-defined algorithms in MATLAB such as "fcm" and "kmeans" which can be used to determine the roll-off factor. These algorithms are mostly used in pattern recognition applications. But these algorithms are not optimum algorithms for the estimation of the roll-off factor. The input to these algorithms is the number of clusters which is the modulation order. Basically, these kinds of algorithms require the knowledge of the modulation type, which is an unknown in our case. So, the focus will be on maximizing the SNR. The method used for roll off factor estimation is based on maximizing the energy of the received signal. This approach may not be the most computationally efficient algorithm but there is no doubt about its efficiency. If the estimation of the symbol rate and the bandwidth is accurate enough, the estimation process of the roll-off factor becomes less computationally complex. The reason is discussed in the previous section, where the estimations of these parameters create a boundary for the roll-off factor.

In the following figures, it can be easily seen that without matched filtering or a wrong matched filtering, i.e. matched filtering with a different roll-off factor, ISI is introduced into the system. The optimum sampling instants are the instants where the eye is widely open. The effect of ISI can be seen at those instants better. Figure 13 shows the eye diagram of a perfectly matched filtered signal and Figure 14 shows the eye diagram of matched filtering process with a different roll-off factor value. If there is no matched

filtering is performed when it is required, Figure 15 is observed. It is easy to note that there is a high ISI and the optimum sampling instant is shifted.

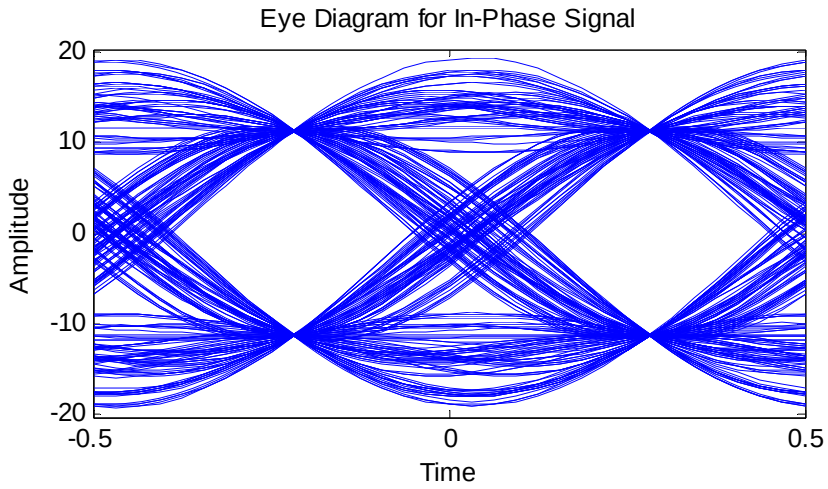

Figure 13: Eye Diagram of In-Phase Component of a 4QAM Signal – Perfect Matched Filtering

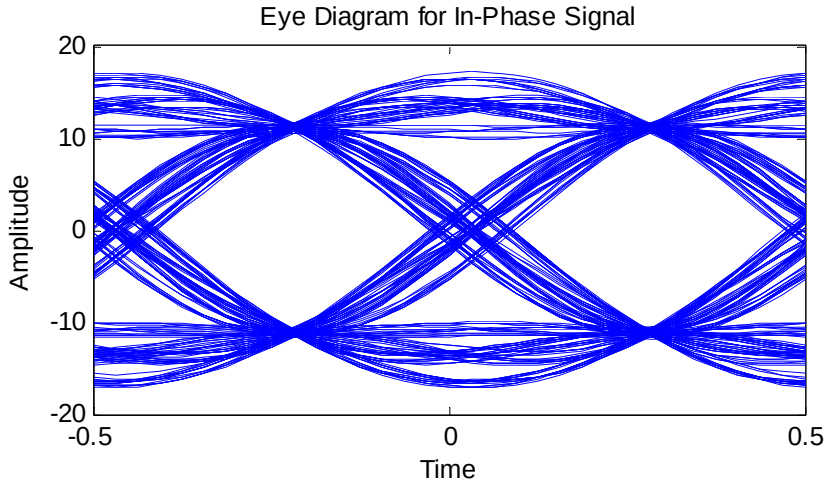

Figure 14: Eye Diagram of In-Phase Component of a 4QAM Signal - Wrong Matched Filtering (Transmitter Roll-off Factor = 0.35 – Receiver Roll-off Factor = 0.50)

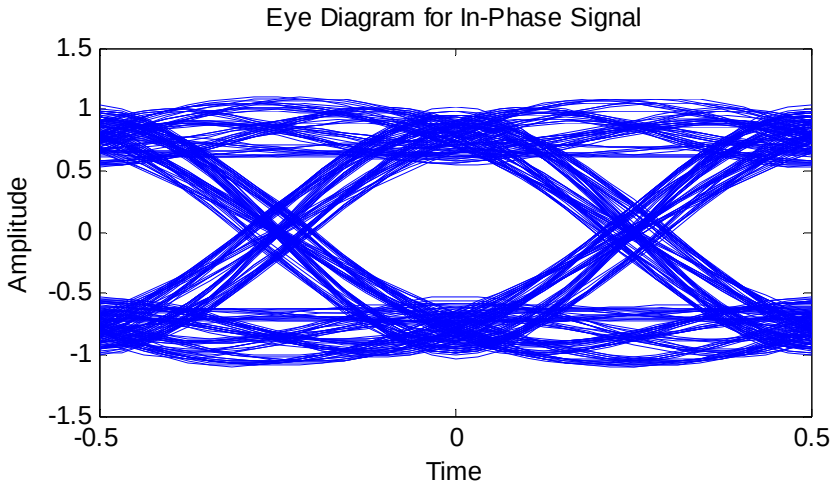

Figure 15: Eye Diagram of In-Phase Component of a 4QAM Signal - No Matched Filtering

4.4. Optimum Sampling Instant Estimation

4.4.1. Challenges

After the match filtering process and the required parameter estimations, the next step is downsampling the signal. Before filtering process at the receiver end, the signal received is already oversampled with an oversampling rate. This oversampling rate is estimated synchronously with the symbol rate and a perfect estimation of oversampling rate is required. This oversampling rate is used first with designing the matched filter and then to downsample the signal. In order to downsample the signal, the detection of optimum sampling instant or in other words optimal sample phase is required. The optimum sampling instant is the instant where the sampling is performed and it has the highest energy and the signal has to be downsampled at this instant. If the signal is downsampled at a different instant, there will be ISI introduced to the system. The effect of the ISI can easily be seen by looking at the eye diagram or the constellation points.

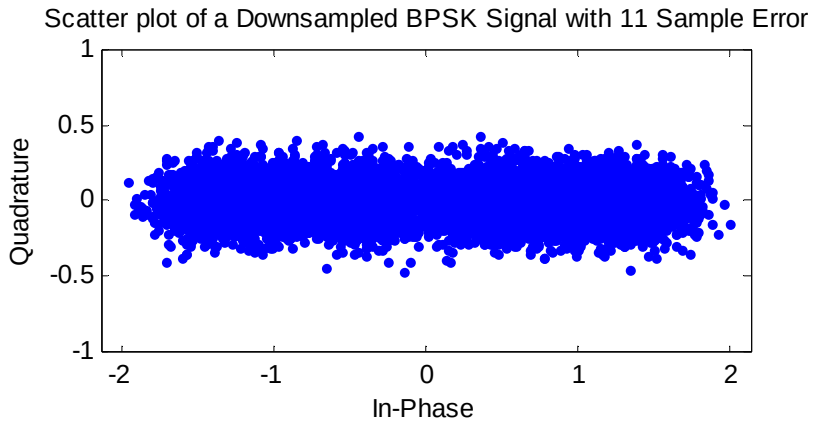

Figure 16: Downsampled BPSK Signal with 11 Sample Errors from the Optimum Sampling Instant

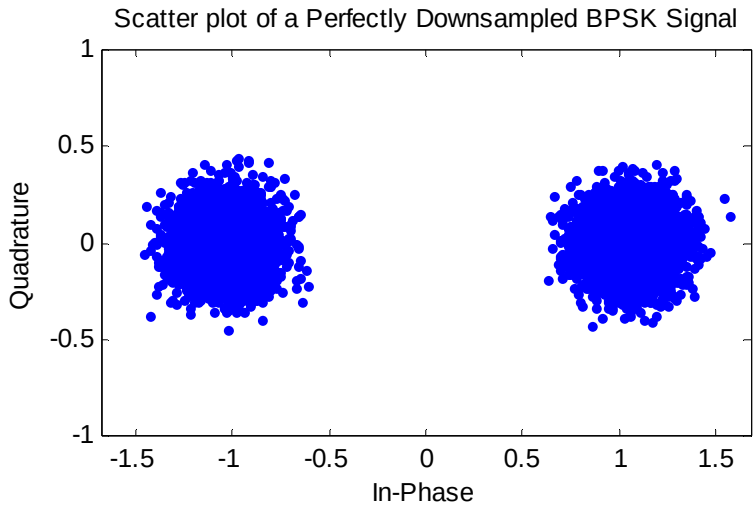

Figure 17: Downsampled BPSK Signal at Optimum Sampling Instant

The estimation of the optimum sampling instant is a key requirement for perfect demodulation as well. If the signal is downsampled at the optimum sampling instant, it will be obvious in the constellation diagrams, which is a visual way to determine the optimum sampling instant. At other instants, the constellation points will be spread around the plot. For example, for BPSK modulation, if there is no frequency and phase offset but slight channel effect, the constellation points will spread between $+A$ and $-A$,

(Figure 16) where A is the magnitude of the received signal. But when the signal is downsampled at the optimum sampling instant, the constellation points will be grouped together. Again for BPSK modulation, if the signal is downsampled at the optimum sampling instant, the constellation diagram will have two groups of constellations, one at $+A$ and one at $-A$ (Figure 17), if there is no frequency or phase offset but slight channel effect. There are two ways to determine the optimum sampling instant. It can be estimated from the eye diagram or from the energy of the signal.

The eye diagram is plotted using the received symbols and eye diagram is a very useful tool in communication systems. In the eye diagram, the symbols are plotted overlapping and while plotting the eye diagram, it is required to take at least 2 symbols at an instant. The eye diagram gives information about the optimum sampling instant and the ISI. The width of vertical eye opening gives information about the ISI, whereas the width of the horizontal eye opening gives some insight about the sensitivity to timing offsets [26]. In raised cosine pulses, which is the case in this study, if a large roll-off factor is used the eye opening is larger. As a result, for small roll-off factors the eye diagram will be more error proneness if the optimum sampling instant is estimated wrong. So, it is important for one to estimate the optimum sampling instant correctly to prevent high errors while using eye diagram. Another consequence in the eye diagram approach results while using higher order modulation types. For BPSK and QPSK the in-phase eye diagram has two levels, which makes our job easier to calculate the distance. In higher order modulation types, there are more levels, which makes the estimation more complex.

Figure 18 shows the eye diagram of the quadrature component of a 16QAM signal. The filter used is a raised cosine filter with a roll-off factor of 0.5. There are four states in an eye diagram of 16QAM meaning that there are four levels for each in-phase component. The optimum sampling instant is shown in Figure 18.

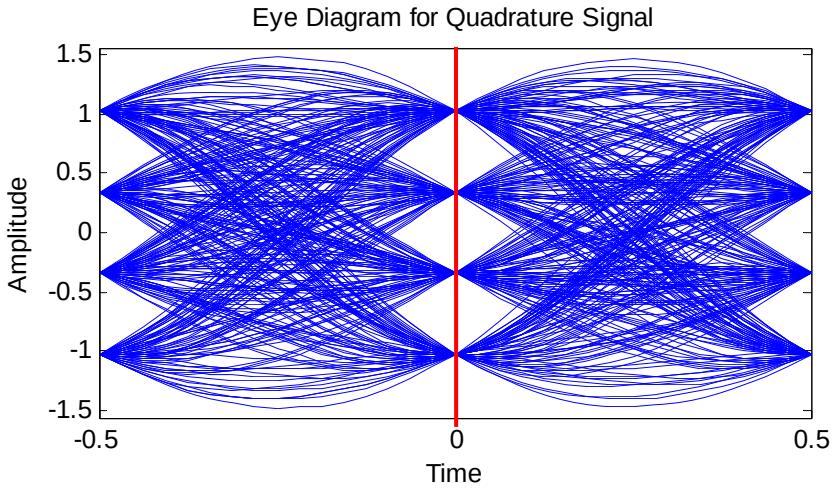

Figure 18: Optimum Sampling Instant for a 16QAM Signal

In order to use eye diagram approach, clustering methods are required, which gives birth to necessity for the modulation order. The closest samples are grouped together and at each sampling instant, the distance is calculated. The instant which has the maximum distance between clusters is the optimum sampling instant. While using the eye diagram approach, it is important to have minimum ISI case. ISI is an important restriction for this approach to be used. If there is high ISI, i.e. wrong matched filtering, then the result of this approach will be misleading. And as stated above, since this approach requires the knowledge of the modulation order it is not acceptable in blind receivers.

4.4.2. Method Proposed

As discussed in the previous section, the clustering methods “fcm” and “kmeans” of MATLAB can be used for the estimation of optimum sampling instant as well. Again, since there is a requirement for the modulation order, this approach is not used in this study.

Another approach for the estimation of the optimum sampling instant is energy based approach, which is based on calculating the total energy at each sampling instant. This technique is less computationally complex with respect to eye diagram approach and proven to be more computationally efficient. As other techniques for optimum sampling instant estimation, the oversampling rate is a key requirement for this case as well. This approach is similar to the approach discussed first. The signal is downsampled at each instant and the energy of the signal is calculated. The instant with more energy is the optimum sampling instant.

This technique is more efficient than other techniques and does not require any other parameter than the oversampling rate. Unlike the eye diagram approach, this approach is efficient for all modulation types. Another important feature of this approach is the number of samples can be limited to reduce the computational complexity.

The estimation of the optimum sampling instant is followed by downsampling the signal. The signal is downsampled at the optimum sampling instant and forwarded to the frequency and phase estimation block.

4.5. Simulation Results

Pulse shape estimation and optimum sampling instant estimation is performed simultaneously. The signal is matched filtered with a roll-off factor and the total energy

of the signal at each instant is calculated. The instant with most energy with a given roll-off factor represents the optimum sampling and the roll-off factor is the roll-off factor used at the transmitter.

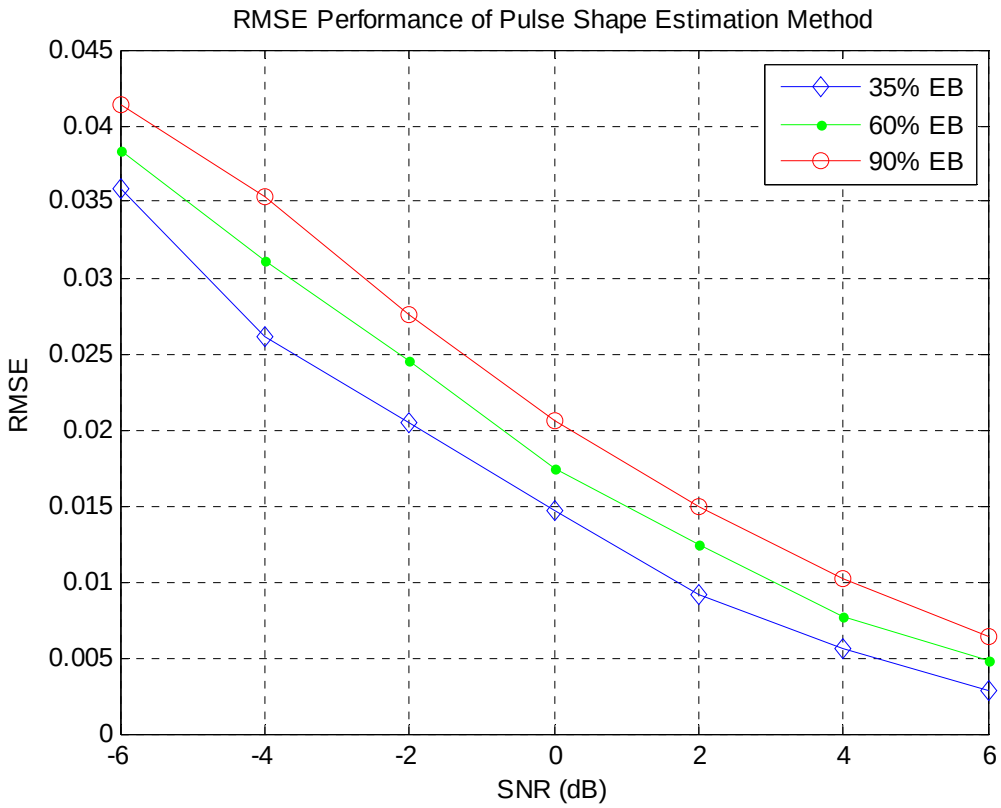

Figure 19: RMSE Performance with Various Excess Bandwidth Conditions

The simulations are performed with a root raised cosine filter having 35%, 60% and 90% excess bandwidth. The proposed methods performance at various SNRs is evaluated and the false alarm rates at various SNRs are provided in Table 1.

With increasing SNR values, the false alarm rates decrease where a false alarm is defined to be a wrong estimation of the roll-off factor. In Figure 19, RMSE performance of the roll-off factor estimation is illustrated. High SNR values yield more close estimations.

Table 1: SNR vs. False Alarm Rate

	-6 dB	-4 dB	-2 dB	0 dB	2 dB	4 dB	6 dB
0.35	23.90%	15.96%	10.94%	6.92%	3.12%	1.28%	0.32%
0.60	25.96%	20.40%	14.84%	9.12%	5.16%	2.18%	0.88%
0.90	29.38%	23.98%	17.16%	11.58%	7.02%	3.66%	1.60%

CHAPTER 5

MODULATION IDENTIFICATION, FREQUENCY OFFSET AND PHASE OFFSET ESTIMATION AND CORRECTION

5.1. Introduction

Frequency offset is caused by the local oscillator mismatches between the transmitter and the receiver and wrong carrier synchronization. There are no two perfect oscillators in the transmitter and receiver which will not cause any frequency offset. So, in each communication system there will be a frequency offset to deal with.

Frequency offset causes a phase rotation in the constellation diagram. Equation 2.3 shows that the amount of rotation introduced to each constellation point is dependent on the sample index and keeps growing. Due to the growing phase rotations, the constellation diagram forms a circular shape. When the signal is downsampled, with a good SNR value and in a flat fading channel, the constellation diagram can be interpreted as rings. The amount of phase rotation between samples is same since the frequency offset value is constant for the entire received signal.

Phase offset is due to the effects of the channel. It also causes a phase rotation in the constellation but different than the frequency offset, the rotation amount is same for all symbols. In Figure 20, a 64QAM constellation under a $\pi/3$ phase offset and $0\ Hz$

frequency offset is illustrated. Usually phase offset is treated simultaneously with the frequency offset.

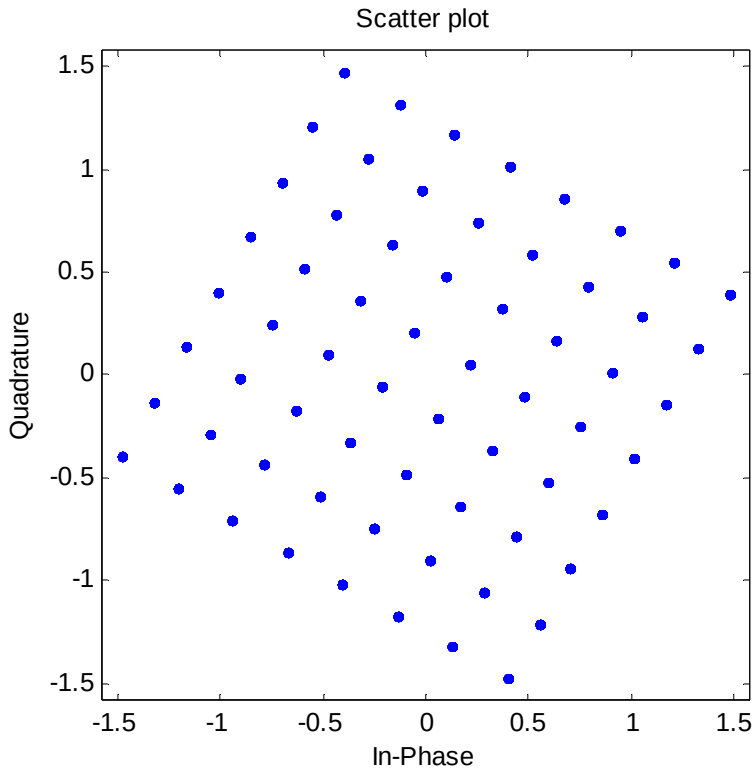

Figure 20: A 64QAM Constellation Affected only by Phase Offset

Frequency offset is a big challenge in receivers. In current receivers there are training sequences such as pre-ambles in North American Digital Cellular (NADC) or mid-ambles in Global System for Mobile Communications (GSM), used to estimate the frequency offset as well as the channel which makes the estimation process easier. In blind receivers, since there is no training sequence is used, frequency offset estimation forms the hardest part. Another problem of frequency offset estimation is the unknown modulation type and modulation order. For example, for PSK signals there is only one amplitude level and different phase levels where as for QAM signals there are different amplitude and phase levels. When QAM types are examined, it is easy to notice that there

are rectangular and circular constellation mappings. For each kind of mapping, it is hard to create a single frequency offset estimation and correction algorithm, so there should be different estimation algorithm for each mapping which gives birth to modulation order estimation.

In Figure 21, constellation diagrams of 4QAM, 16QAM, 32QAM and 64QAM are given. When the signal power is good, number of rings can be easily distinguished by inspecting the PDF of the amplitudes.

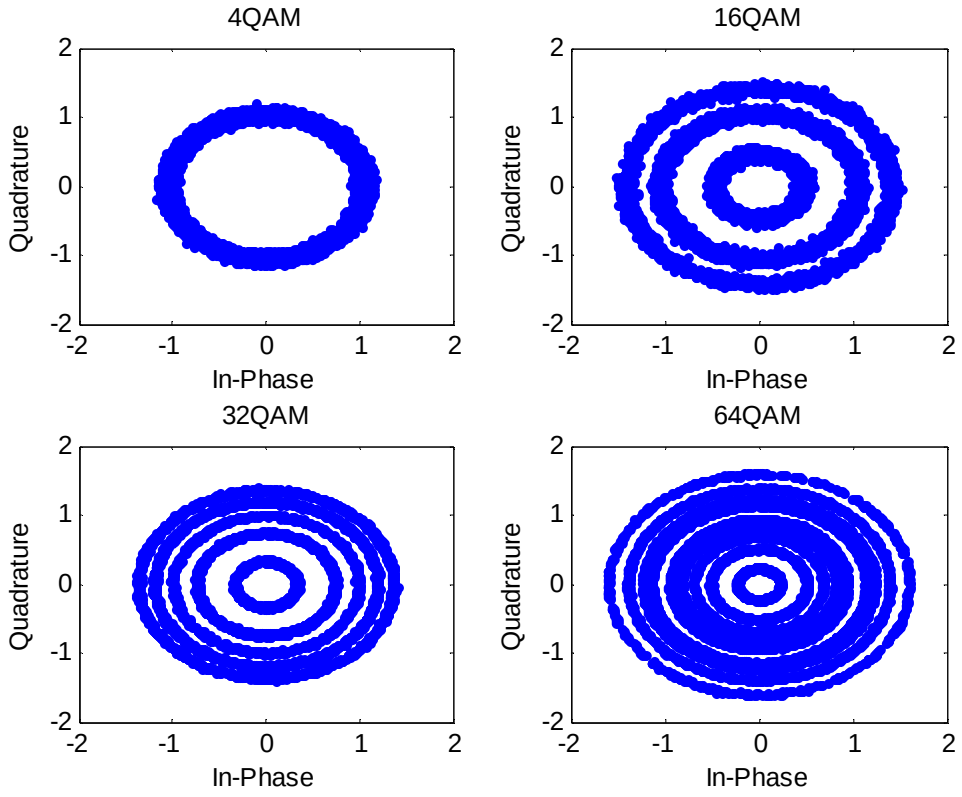

Figure 21: Constellations Diagram after Downsampling

The modulation order can be estimated by counting the number of rings which would work perfectly if only rectangular mappings are considered. For example, in 16QAM rectangular constellation there are three rings and in a rectangular constellation of 32QAM there are five rings after downsampling process in a slightly dispersive

channel. If the circular constellations are considered, the things will not work out smoothly. 16QAM has 4 different well known constellations as shown in Figure 22. It is easy to note that, even for different mappings of a single modulation type there are same amount of rings. To exactly determine the correct modulation order and mapping, the probability density function (PDF) of the received constellations and the information of distance between the rings should be used.

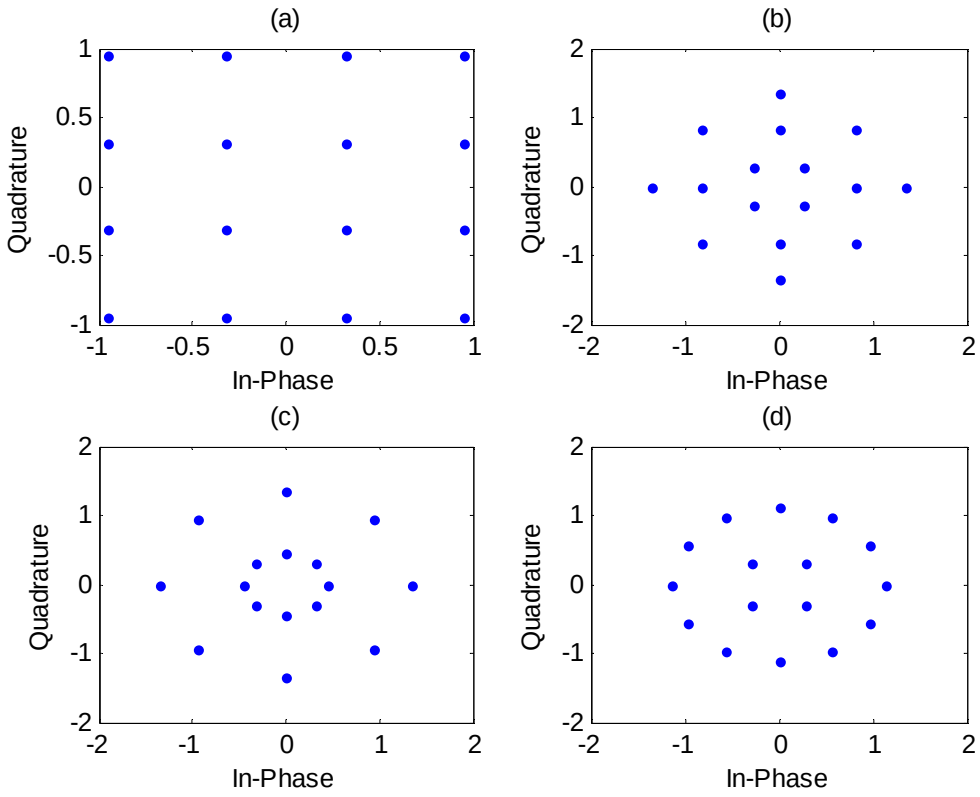

Figure 22: Different 16QAM Constellations. (a) (4, 8, 4)

(b) (4, 4, 4, 4) (c) (8, 8) (d) (4, 12)

When noise and frequency offset is introduced to the constellation diagrams in Figure 22, Figure 23 is obtained. The densities of the constellations depend on how many symbols a ring contains. For example, Figure 22(a) represent the rectangular constellation diagram of 16QAM and it consists of three rings. There are 4, 8 and 4 constellations in

the inner, middle and outer ring respectively. Figures 22 (c) and (d) both have 2 rings but they have different PDFs.

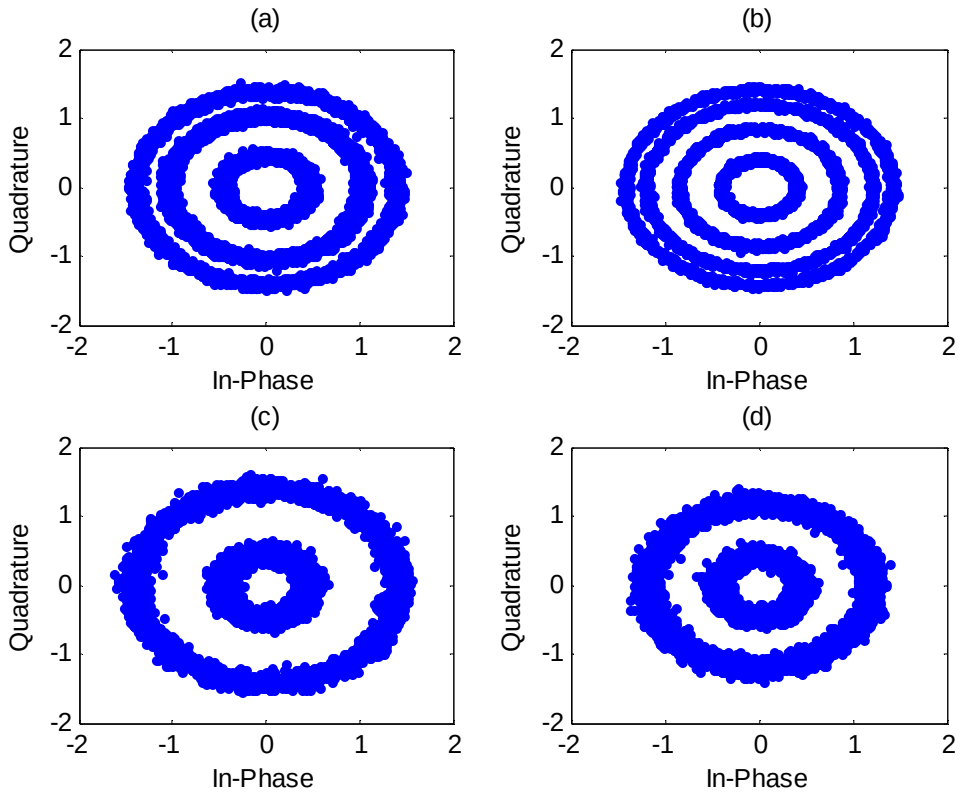

Figure 23: Different 16QAM Constellations with Frequency Offset. (a) (4, 8, 4) (b) (4, 4, 4, 4) (c) (8, 8) (d) (4, 12)

In Figure 24, the PDF of rectangular 16QAM constellation is represented. Horizontal axis is the amplitude distribution of the received symbols. The densities of first and third rings are roughly the same and the density of the second ring is two times this density. Red lines denote the clusters. As the method suggests, some of the clusters are close to each other and these clusters are grouped together and form a centroid location.

The biggest challenge arises when the frequency offset is larger than the symbol rate. If the frequency offset value is too high, a rough estimation of frequency offset

should be done, which is a feed-forward step. By employing a feed-forward algorithm the high frequency offset is removed and it is tracked with a feed-back algorithm which all dependent on Phase-Locked Loops (PLLs). Each of the PLL algorithms in the literature assumes that the modulation order is known, i.e. they are designed to work with some standard.

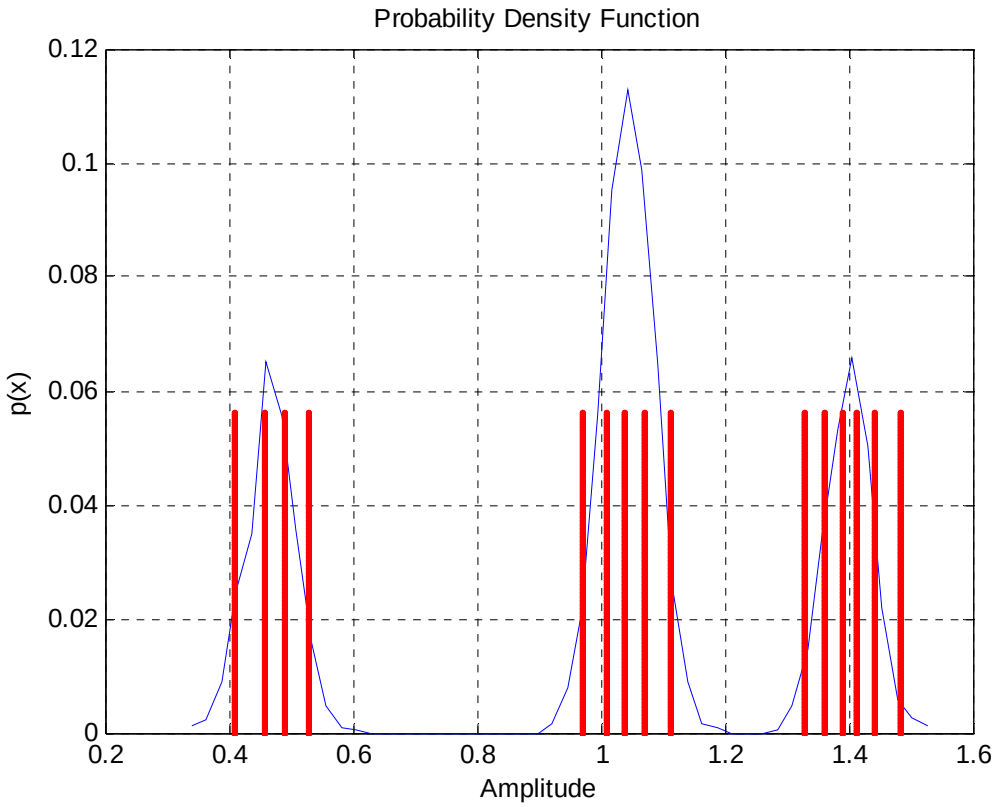

Figure 24: Probability Density Function of the Rectangular 16QAM Constellation

5.1.1. Literature Overview and Challenges for Frequency Offset and Phase Offset

The frequency offset and phase problem is widely studied in the literature and they are treated jointly. There are some data aided and non-data aided methods proposed for the estimation process. This work focuses on the non-data aided frequency offset estimation as a part of blind receivers. The frequency offset estimation can be done in two ways; feed-forward and feed-back. Feed-forward algorithms remove the high

frequency offset and feed-back algorithms correct the remaining residual errors. There are two kinds of feed-forward algorithms. One of them is a cyclostationary based approach whereas the other approach depends on the sample correlations.

The basics of the feed-forward algorithms are founded by Viterbi in 1983 [27]. The method estimates the frequency offset using the cyclostationary features of the signal. The usual cyclostationary process takes the signal and multiplies it with the delayed conjugate of itself and finds the Fourier coefficients. At a cyclic frequency α, there is a spectral line which can denote the symbol rate, carrier frequency or the frequency offset. According to Viterbi, for an MPSK signal, if the signal is raised to M^{th} power, there will be a spectral line generated at $\alpha = Mf$, where M is the modulation order, f is the frequency bin where the spectral line generated and f_N is the frequency offset. The frequency offset estimation equation is given by,

$$\widehat{f_N} = arg\ max_f \left\| \frac{1}{N} \sum_{n=0}^{N-1} y^M(n) e^{-j2\pi(Mf)n} \right\|^2 \qquad (5.1)$$

This equation holds for M-ary PSK signals. For QAM signals, Serpedin et al. [28] proved that this equation holds in the 4^{th} order, and the equation can be written as

$$\widehat{f_N} = arg\ max_f \left\| \frac{1}{N} \sum_{n=0}^{N-1} y^4(n) e^{-j2\pi(4f)n} \right\|^2 \qquad (5.2)$$

The spectral line is generated using the 4^{th} power of the received signal for any MQAM modulation type. At $\alpha = 4f$ there is a dominant spectral line which is caused due to the frequency offset. Using this cyclostationary process, the frequency offset is estimated and it is removed from the signal. But still there is some residual frequency offset and keeps growing as the sample index increases as can be seen from equation 2.3.

Cyclostationary based approaches are computationally complex algorithms. In each frequency bin in the interval $(-\frac{f_s}{2}, \frac{f_s}{2}]$, the sum should be calculated and the maximum of these results denotes the frequency offset. In order to decrease the computational complexity a rough idea about frequency offset should be known.

Another feed-forward frequency offset algorithm depends on the sample correlations separated by the symbol period assuming that channel does not change or changes a little between these two symbols [29]. The signal is multiplied by a delayed conjugate version of itself, i.e.

$$x(t) = r(t)r^*(t-T) \qquad (5.3)$$

This process will generate a fundamental tone at $f = 1/T$ and the phase of this fundamental tone may be used to extract the frequency offset and the optimum sampling instant information. The frequency offset information is contained in the periodic components of this signal.

These feed-forward frequency offset estimation algorithms do not yield to robust results. They should be followed by a feed-back frequency offset estimation algorithm. In this work, the frequency offset in the system is supposed to be well below the symbol rate of the received signal, so only feed-back frequency offset algorithm will be used.

Feed-back frequency offset algorithms depend on PLLs. These kinds of algorithms estimate the frequency offset for each sample and correct the frequency offset of the following sample by using this estimation. To prevent residual errors growing, this method is a promising solution. There are decision-directed PLL algorithms which work well with low order QAM. With the increasing order of QAM, the performance degrades because of the decision errors. Another proposed method is reduced constellation method

which only considers the outermost 4 constellations, i.e. constellations having the highest SNR value. Since they have the longest radius, they can be referred as constellations having highest SNR. The major drawback of this algorithm is for higher order QAM the probability of getting a constellation in the desired region is very low. Instead of taking only the constellations with highest SNR, Sari and Moridi [30] proposed an algorithm which considers the symbols in the diagonal, i.e. symbols having a phase of $\pi/4$. This algorithm is not very effective due to the sensitivity of inner constellation points to the noise, which will yield false estimation results. Another proposed algorithm is a polarity decision phase detector algorithm. The algorithm has higher complexity issues since there is a requirement for loop filter to change the bandwidth of the signal. In this section, these algorithms will be discussed in detail.

The reduced constellation method proposed by Jablon [5], consists of a phase discriminator, loop filter and voltage controlled oscillator. In this method, the outermost four constellation points are taken into consideration. For this purpose a threshold value is defined at the phase discriminator part and these constellation points are chosen to be used. If the magnitude of the received symbol is larger than the threshold, i.e. if it is one of the outermost four constellations, phase discriminator function is performed; otherwise the output of the phase discriminator is set to zero. Using these constellation points the algorithm detects the phase errors.

The method proposed by Kim and Choi [31] is a polarity decision phase detector algorithm. The algorithm assumes that the symbol timing of the signal is perfectly established. Suppose a received signal $q(n)$. If the signals' amplitude $|q(n)|$ is larger than a previously defined threshold τ, the phase detector performs a polarity

decision, $p(n)$, otherwise the signal is not passed through to the polarity detector. The polarity decision depends on the quadrant of the received symbols and using the received symbol and the polarity decision the error signal is generated. The error signal is;

$$\varphi(n) = Im\left[\frac{q(n)}{p(n)}\right] \qquad (5.4)$$

where Im represents the imaginary part. Using the error signal generated, the phase rotation of the constellation is performed. After coarsely synchronizing the frequency, the system is switched into a fine mode and the synchronization is performed in this step as well. In the final step, the algorithm runs in decision directed mode. The complexity of this algorithm is high since it operates in high number of modes and each mode has different set of parameters.

Ouyang et al. [32] proposed a joint phase and carrier recovery algorithm based on the method proposed by Kim and Choi. This algorithm has the same phase detector part as the previous algorithm. The remaining parts of the algorithm are phase offset estimator and frequency offset estimator. The frequency offset estimator block starts with track and hold. The phase is tracked up to some point to operate away from the boundaries. In each step a frequency offset (CF) is calculated using a variable step size controller (VSSC). The step size changes according to the sign of the tracker output. If the sign change consecutively twice, step size (SF) is halved where as if it does not change consecutively twice step size is doubled and added or subtracted from the previous estimation of frequency offset. When it changes consecutively twice, it means that the estimation is close to the frequency offset, which means that the frequency synchronization is being achieved.

$$CF_i = CF_{i-1} + SF_{i-1}sgn(average\ of\ tracker\ output) \qquad (5.5)$$

One of the recent papers published in this area is a polarity decision stop and go algorithm [33]. The polarity detection of the received symbol is performed and error signal is generated. Then, this error signal is fed into a stop and go block. This block compares the sign of the current and previous error signals and generates a new error signal to compensate the phase rotation. This algorithm can be employed to QAM signals without using a power detector to eliminate the inner constellation points.

All the methods summarized in this section require the knowledge of the modulation type and designed for some specific standards. In the following section, modulation identification methods will be described and in Section 5.2, a joint modulation identification and frequency and phase offset correction method will be proposed.

5.1.2. Literature Overview and Challenges for Modulation Identification

Blind modulation identification is widely studied in the literature and there are some methods proposed to overcome blind modulation identification problem. Moment based, cumulant based, wavelet transform based and neural networks based algorithms are mostly used for blind modulation identification.

In moment based approaches, modulation identification is performed through inspecting the higher order statistics of the signal. In order to compare the signals, the mean (first order statistics) of the signal is set to zero or the second order statistic, which is the variance, is normalized to one. By inspecting the higher order statistics, the behaviors of the signals are determined. Cumulant based approaches are derived from the moment based approaches. Both of the approaches perform well in high SNR cases and in AWGN channels. The algorithm can discriminate between MPSK signals, lower order

MQAM signals and also can discriminate if the signal is modulated with FSK [34, 35 and 36].

Inspecting instantaneous amplitude, phase and frequency changes is another identification method. PSK and FSK modulated signals have constant amplitudes where as QAM signals have more than one amplitude level. As their names imply, FSK and PSK modulations includes frequency and phase information respectively. On the other hand, QAM signals includes both phase and amplitude information. If the channel effect is less or it is equalized, by the information gained through PDF of the amplitude, the discrimination can be made between QAM, FSK and PSK signals. Throughout simulations, it is observed that FSK has less amplitude variance with respect to other modulation types. If the channel degradation is less, PSK signals will have less variance than the QAM signals. To detect the order of PSK and FSK signals, phase and frequency change information of the signals should be inspected [37].

Wavelet transform is another method for modulation identification. Haar wavelets are used with received signal and the orders of FSK signals can be identified by inspecting the side lobes [38, 39].

Sometimes the algorithms are combined together and in a decision based way the modulation identification is performed. This kind of identification is called neural networks based modulation identification. The performance of neural network based approach is significantly better since there is more than one method used for the problem.

In the literature, modulation identification can be made using the methods outlined in this section. The performance of the methods is affected by the SNR, number of channel taps and the offsets such as frequency and phase.

5.2. Method Proposed

In this work only QAM signals are considered. As stated previously, QAM signals may have different constellation mappings; rectangular and circular. In order to correct the frequency offset, first; modulation order and constellation will be detected. In order to detect the modulation order, the information of number of rings in the constellation, the PDF of the symbols and the distance between rings may be used. Figure 25 shows the block diagram of joint modulation identification and phase offset and frequency offset correction. Modulation identification is followed by phase offset correction, and the algorithm finishes with frequency offset correction.

The considered constellation mapping in this work is only rectangular. But still there is a need for modulation order detection. For rectangular mappings, the number of rings for each modulation order is unique. So, the information gained by number of rings is enough for modulation order detection. K-means clustering algorithm is used to find number of rings. This algorithm is generally used for pattern recognition algorithms in computer science. There is a need for number of clusters to be found and is chosen to be fifteen since the k-means method sometimes misclassifies the data points and creates close clusters. In order to find all the centroid locations there should be more clusters than needed and it should be followed by a cluster classifier method, which will be discussed next. The k-means clustering algorithm will find fifteen centroids for the clusters based on the amplitude of the downsampled data. This method is used to determine which cluster the data belongs to. In each step the centroid locations and the distance of each data point to these centroid locations is calculated. The algorithm assigns each data point

to the centroid of closest distance, and calculates the new centroid location. When the procedure converges, the algorithm stops and centroid locations are determined.

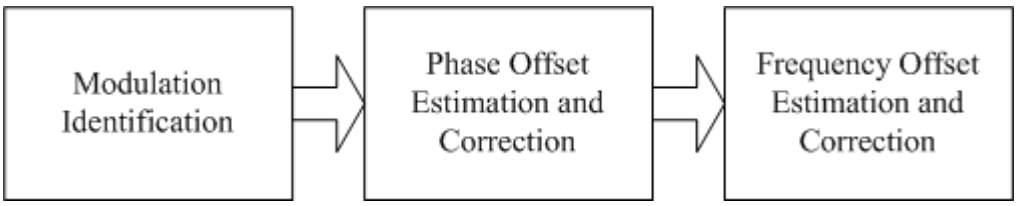

Figure 25: Proposed Method

In some modulation orders there will be more clusters than needed. In order to distinguish if each cluster is unique a basic method is used. The method depends on the distances between clusters. If the distance between two clusters is less than a threshold then they are grouped together and they form a single cluster. After this process the modulation order is determined and the symbols are fed into the frequency estimation block.

After the modulation identification, first the phase offset of the received signal is estimated and corrected in a feed-forward way then frequency offset estimation and correction is performed.

The first block in phase offset estimation is an energy detector which selects the outermost constellations. Also, there is a safe region defined because the noise may shift symbols to the next quadrant or to the other half of the quadrants which will yield false results. The phase rotation of these symbols is calculated in the second block and the phase differences are observed. When there is a phase offset is present in the system, all the symbols are rotated with same amount. Let $r(k)$ denote first symbol in the safe region which successfully passed the energy detector and let $\varphi(k)$ denote the phase of this symbol.

The phase rotation due to the frequency and phase offsets are given in equation 4.8. The phase rotation, $\emptyset(k)$, due to the frequency offset can be ignored due to its small effect.

$$\emptyset(k) = \varphi(k) - \frac{\pi}{4} = 2\pi f_o k T_s + \theta \cong \theta \qquad (5.6)$$

where $|2\pi f_o k T_s| < \pi/4$ and k is the symbol index.

So, from equation 4.8 the phase of $r(k)$ represents the phase offset. In order to have precise estimation of phase offset, a set of symbols should be inspected. The used symbols for phase offset estimation are the symbols that do not have a phase rotation larger then $\pi/4$.

For QAM constellations mapped in a rectangular manner, the proposed frequency estimation method starts with an energy detection block, i.e. the constellations with highest SNRs are chosen. A threshold is defined based on the received signal. A block diagram of the frequency and phase offset estimation method can be found in Figure 25. These constellations are known to have a phase of $\pi/4$ if the synchronization is perfect. By inspecting the phase rotation of these symbols it is straightforward to have a frequency offset value. The estimations for the frequency offset are only made using the outermost constellations. If the received symbol cannot pass the energy detection, the previously estimated frequency offset will be used to correct the following symbols until a new coming symbol successfully passes the energy detector.

The next step is mapping all the received symbols into the first quadrant. If all the symbols are in the first quadrant, an increasing or decreasing phase change is expected. The phase difference between the received symbols' phase and $\pi/4$ represents the effect of frequency offset to that symbol. If the frequency offset value is small, the amount of

phase rotation of first symbols denotes the phase offset in the system. By manipulating the phase rotation (4.9), an estimation of frequency is obtained. This obtained value is used to correct the frequency offset of the following symbol. This is a feed-back method which works like the polarity detection methods.

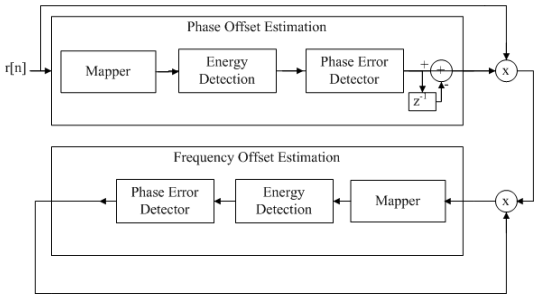

Figure 26: Joint Phase and Frequency Offset Correction

The frequency offset f_o is estimated through the n^{th} symbol is given by,

$$f_o(n) = \frac{\emptyset(n) f_{symbol}}{2\pi n} \qquad (5.7)$$

where $\emptyset(n), n$ and f_{symbol} denote the phase rotation of the n^{th} symbol, symbol index after downsampling and symbol rate respectively. And the frequency offset of the consecutive symbol is corrected by using the estimated frequency offset (Equation 5.8).

$$r(n+1) = r(n+1)e^{j2\pi f_o(n)(n+1)T_s} \qquad (5.8)$$

Figure 26 shows a 16QAM signal with positive frequency offset. The phase difference between constellations and $\pi/4$ radians is illustrated. When there is an increase, a symbol having a magnitude larger than threshold is arrived and an estimation of frequency offset is performed. If it is stable after an increase, it means that the received symbol has a magnitude smaller than the threshold value defined. When there is a fall from $\pi/4$ to -$\pi/4$ radians, the quadrant has changed. In order to have a good estimation, these plots have to be increasing all the time since the phase difference is growing as

sample index increases. Figure 27 is expected to rise smoothly when the modulation order is 4QAM. When the modulation order increases, since the probability of getting a constellation larger than the threshold value decreases, the continuous increase will be broken down.

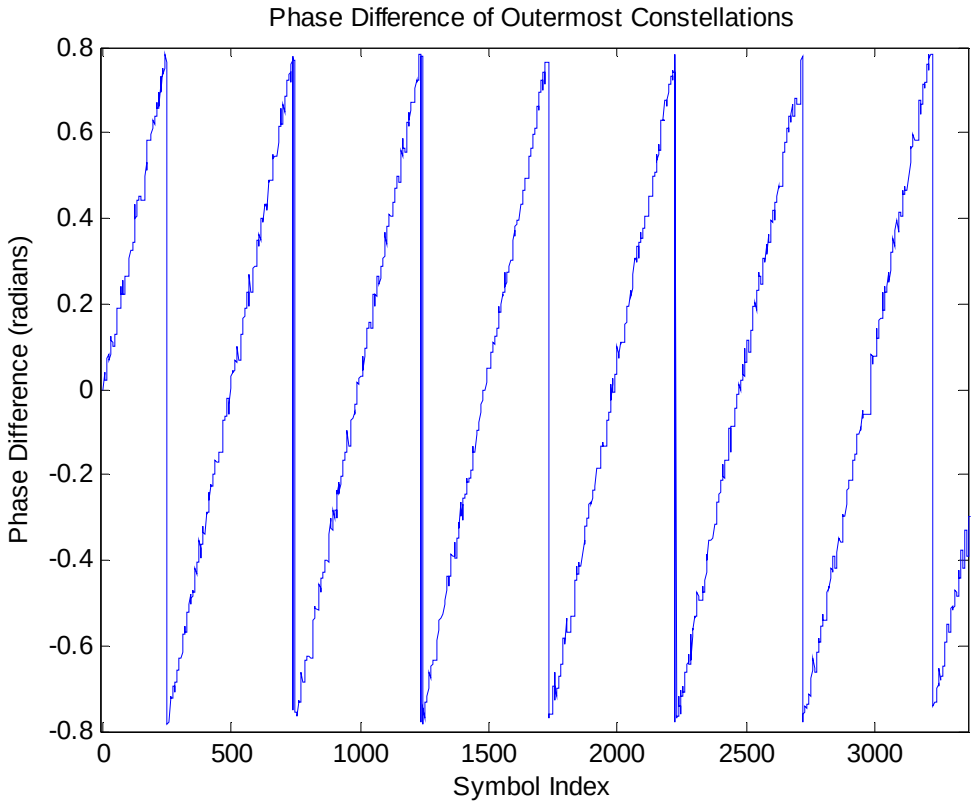

Figure 27: 16QAM Signal with a Positive Frequency Offset

The major challenge in this method arises when the symbols cross the boundaries, i.e. horizontal and vertical axes. Suppose a positive frequency offset rotating the symbol constellations counter-clockwise. When the phase rotation caused by the frequency offset is larger than $\pi/4$, the symbol will pass to the second quadrant, which will be mapped to the first part of the first quadrant, i.e. all symbols in the second quadrant will be rotated $\pi/2$ radians in the clockwise direction, symbols in third quadrant will be rotated $3\pi/2$ radians in the clockwise direction, etc. As stated above, the phase difference

with respect to the constellations on diagonal will change between $[\pi/4, -\pi/4]$, but it is expected to be growing all the time. So, when the phase difference moves from a positive

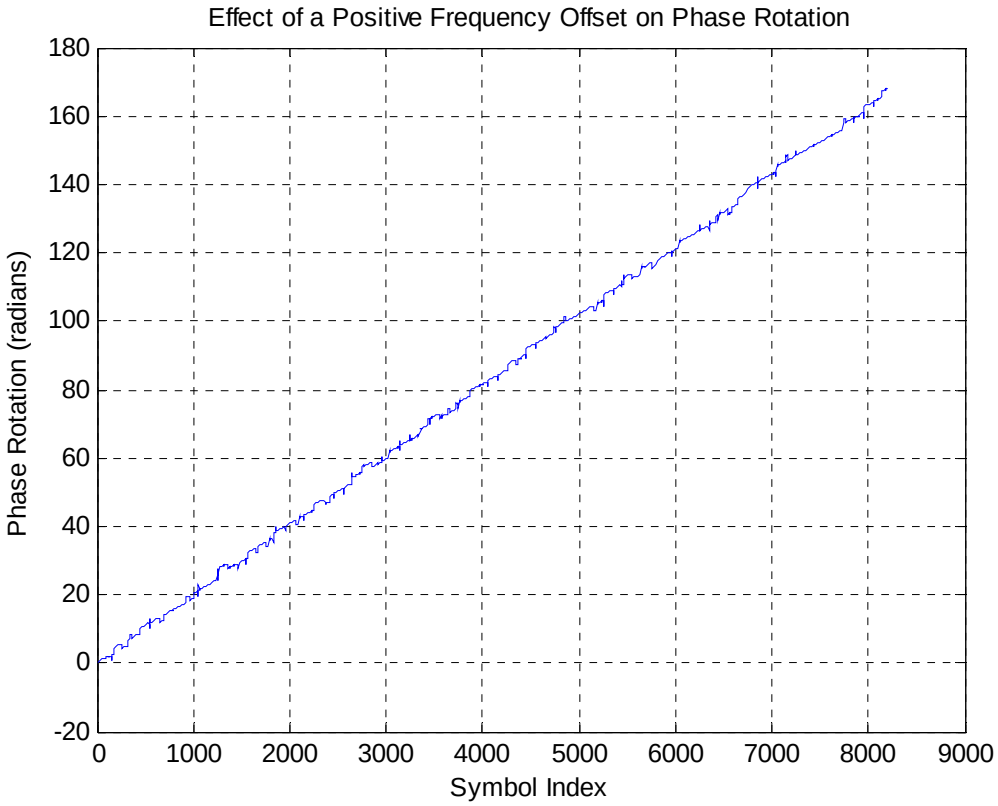

Figure 28: Phase Rotation Tracking

value to negative value, or vice versa, which means that there is a quadrant change, $\pi/2$ should be added to the phase difference value in order to keep it growing. When quadrant changes for the second time, $\pi/2$ will be added to the phase difference value, and it is followed by in the same manner. Figure 28 is obtained after doing the proposed additions which is expected since the phase rotation is always growing (in a positive frequency offset case).

Figure 29 shows the constellation diagram after mapping all symbols to first quadrant in blue and the threshold value in red. The constellation points remaining outside the threshold are referred as the symbols having the highest SNR value. For

frequency and phase offset estimations, if the received symbol has a magnitude higher than the threshold value, it is going to be used for the estimation otherwise, there will be no action taken.

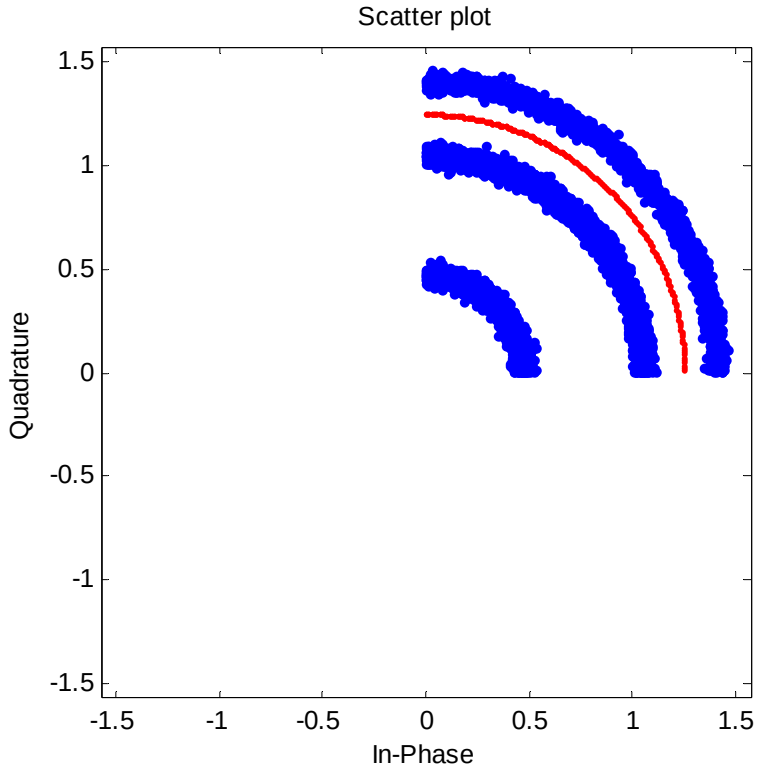

Figure 29: Constellation Diagram after Mapping all Symbols to the First Quadrant

For a non-square constellation mapping of QAM, i.e. 8QAM, 32QAM and 128QAM, the process is similar. For these types of constellations, the symbols considered are the constellations having the highest SNR value. In a higher order non-square constellation case, there are eight constellation points to be considered. In Figure 31, this method is illustrated. The constellations which are outside the red circle (threshold) are chosen to estimate the frequency offset. Starting from the first symbol, each symbol is passed through an energy detector and if their energies are higher than a threshold value they are passed through the frequency offset estimation block.

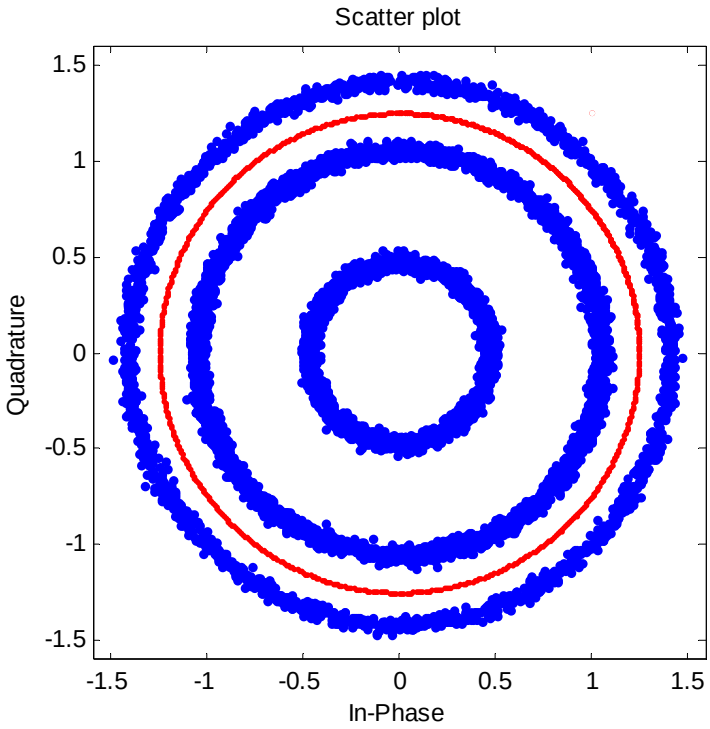

Figure 30: Representation of Threshold Value

5.3. Simulation Results

The simulations are performed with various QAM modulation orders. First, the modulation type and constellation mapping of the received symbol sequence is determined. Based on the downsampled signal, the PDF of signal amplitudes is obtained. Then clustering methods are used. The number of clusters used is chosen to be fifteen since having higher number of clusters than needed gets rid of the deficiencies of the method used. For example, if the modulation type used is a 16QAM with rectangular mapped constellations, there will be three groups of constellations. Depending on the distances between clusters, close clusters will be grouped together. The number of clusters yields to the modulation order used at the transmitter. The false alarm rates for modulation identification technique are given in Table 2. The simulations are performed

at 30 dB SNR with eleven and fifteen clusters. When the cluster number increases, the performance of higher order QAMs also increases. The frequency offset estimation algorithm block will choose one of the two estimation algorithms depending on the modulation order; one designed for square constellations (i.e. 16QAM) and the other designed for non-square constellations (i.e. 32QAM).

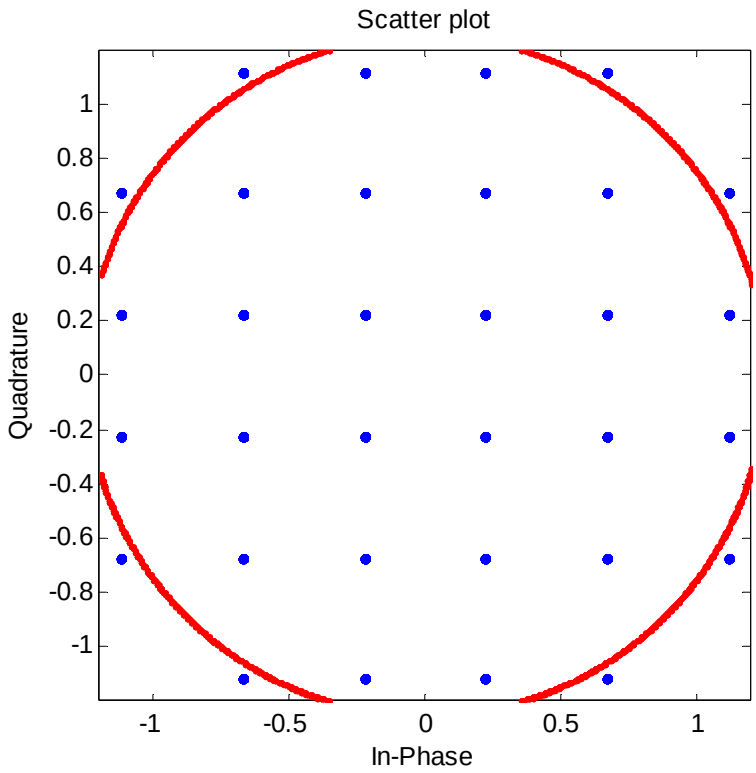

Figure 31: Useful Constellations of 32QAM

The performance of the frequency offset estimation algorithms depends on the ratio between the frequency offset value and the symbol rate and the modulation order. For example, the acquisition range of 16QAM will be higher than 64QAM. This is due to the proposed method's energy detection approach. The probability of getting a symbol outside the threshold value will decrease as the modulation order increases.

Table 2: False Alarm Rate of Modulation Identification Technique Proposed

	11 Clusters	15 Clusters
16QAM	0%	0%
32QAM	1%	0%
64QAM	12%	1%

Figure 32 shows the frequency and phase offset tracking for a 16QAM signal with a symbol rate of $100\ kSps$ and a frequency offset of $1\ kHz$ at $20dB$. In Figure 33, the constellation diagram after the frequency offset correction can be seen. The constellation points are mapped to the original locations. When there is a constellation higher than the threshold, the phase difference is increasing (or decreasing if there is a negative frequency offset) otherwise, it keeps constant which can be seen in Figure 28 when closely inspected. After some amount of symbols processed, frequency offset converges and fluctuates around the frequency offset value.

In Figures 32 and 34, the fluctuations at the beginning of the estimation are caused by the effect of noise to those constellations. These constellations are close to boundaries and an affect of noise may push them beyond the boundaries. There is a trade-off between the safe region and the estimation performance. If the safe region is increased to remove high frequency estimation errors after the estimation algorithm starts, then tracking of the frequency offset will be performed very late which will cause more errors.

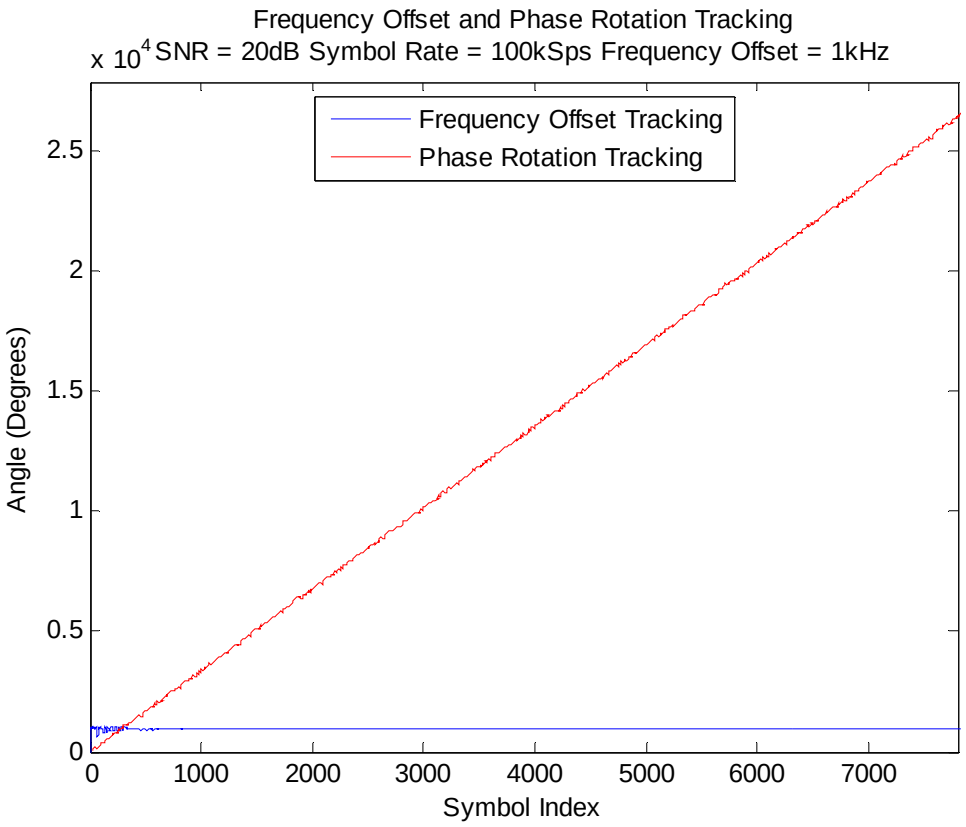

Figure 32: Frequency Offset and Phase Rotation Tracking for 16QAM

Figure 33 and 35 are the constellation diagrams after the frequency offset correction. The scattered constellations around the dense constellations are due to the wrong estimation of the frequency offset in the beginning.

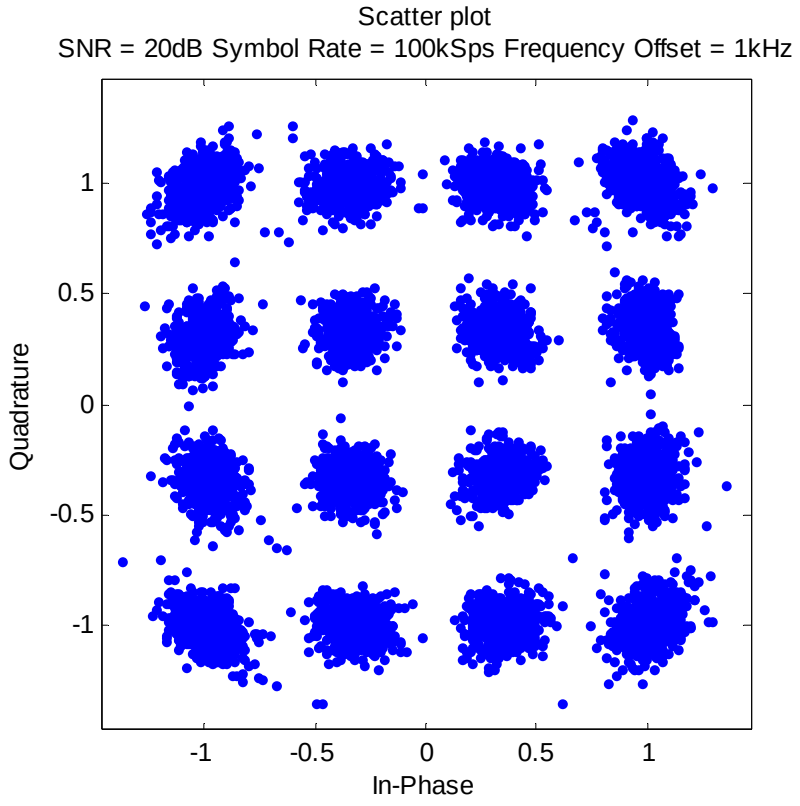

Figure 33: Constellation Diagram of a 16QAM Signal after Frequency Offset Correction

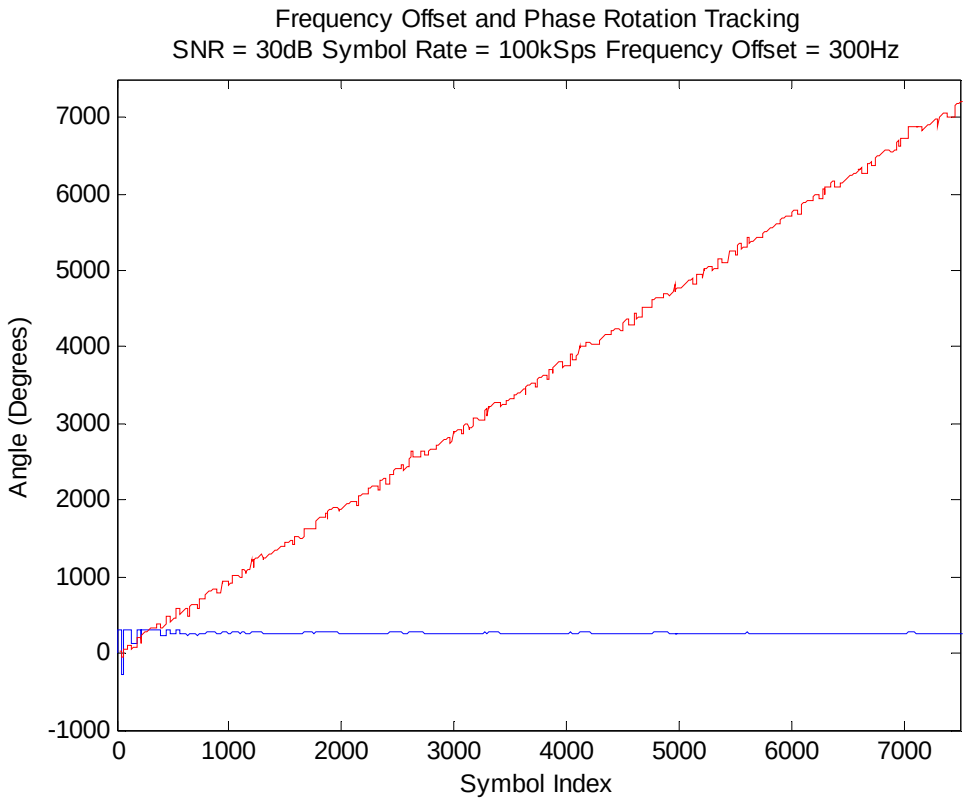

Figure 34: Frequency Offset and Phase Rotation Tracking for 64QAM

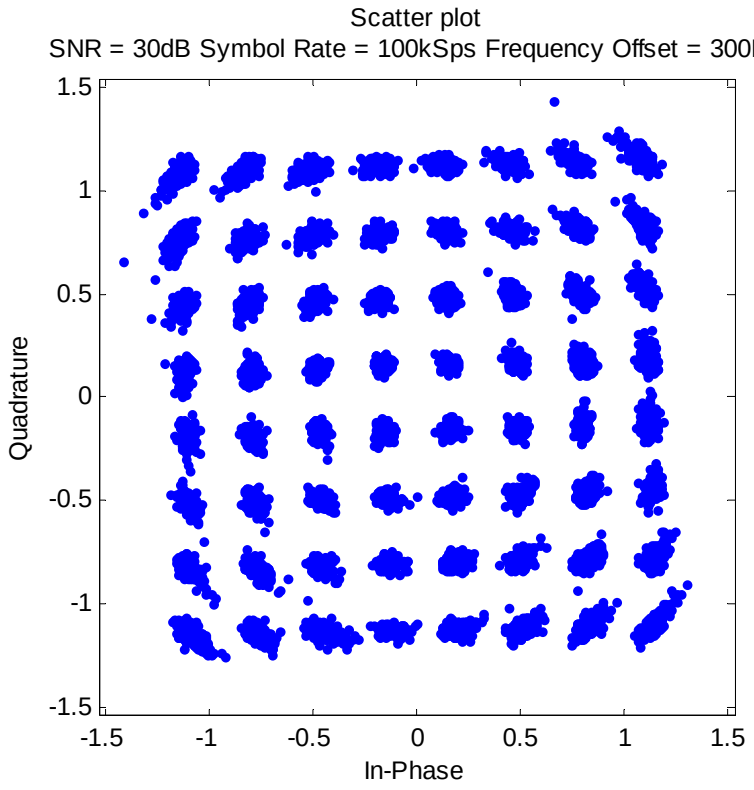

Figure 35: Constellation Diagram of a 64QAM Signal after Frequency Offset Correction

CHAPTER 6

SUMMARY AND CONCLUSIONS

6.1. Contributions

This study proposes a fully blind receiver for cognitive radio and public safety applications. In the literature, there is no solid work on bandwidth and carrier frequency estimations. A simple algorithm for these parameters is proposed. Non-data aided symbol rate estimation problem is widely studied in the literature. The proposed methods are coarse or fine estimation methods and fully blind symbol rate estimation does not exist in the literature. The proposed method includes coarse and fine estimation steps. The coarse estimation step shows a significant improvement over the ones available in the literature. The advantage gained from the coarse estimation step is used in the fine estimation step. Roll-off factor estimation is an open area and has not been studied extensively. The proposed approach estimates the roll-off factor jointly with the optimum sampling instant and this method is based on maximizing the SNR of the matched filter output. The last part of the blind receiver which is the modulation identification and phase and frequency offset estimation part is extensively studied. Modulation identification techniques work for specific types and they require the channel to be flat and no frequency offset is introduced into the system. The joint frequency and phase offset estimation techniques require the knowledge of the modulation type and order. The proposed method first estimates the modulation order for QAM signals and by using a suitable algorithm for

square and non-square constellation mappings, the phase and frequency offset is estimated and corrected.

6.2. Conclusions

Cognitive radios are future wireless devices and they are promising solutions for spectral crowding and opportunistic spectrum usage. Cognitive radios' coexistence property suggests that each radio in the spectrum can sense each other and demodulate incoming signals and respond them using their own parameters. In this sense, blind receivers are very important and the blind receiver concept and its steps are explained in detail. Especially in public safety cases, cognitive radios are very important. Another important feature of blind receivers is since they do not use pilot sequences, and they are spectrally efficient because of this property. The estimation methods for the blind receivers' unknown parameters are discussed and brief literature overview is given. Computer simulation results for proposed methods are provided. The purpose of this study is to highlight the importance of blind receivers in wireless communications and cognitive radios.

REFERENCES

[1] S. Haykin, "Cognitive radio: brain-empowered wireless communications," IEEE J. on Selected Areas in Commun., vol. 23, no. 2, pp. 201-220, Feb. 2005.

[2] J. Mitola, “Cognitive radio for flexible mobile multimedia communications,” in Proc. IEEE Int. Workshop on Mobile Multimedia Commun. (MoMuC ’99), Nov. 1999, pp. 3–10.

[3] K. Mueller and M. Muller, "Timing Recovery in Digital Synchronous Data Receivers," IEEE Trans. on Commun., vol. 24, no. 5, pp. 516-531, May 1976.

[4] F. Gardner, "A BPSK/QPSK Timing-Error Detector for Sampled Receivers," IEEE Trans. on Commun., vol. 34, no. 5, pp. 423-429, May 1986.

[5] N.K. Jablon, "Joint blind equalization, carrier recovery and timing recovery for high-order QAM signal constellations," IEEE Trans. on Sig. Process, vol. 40, no. 6, pp. 1383-1398, June 1992.

[6] Y.T. Chan, J.W. Plews, and K.C. Ho, “Symbol rate estimation by the wavelet transform,” in Proc. IEEE Int. Symp. on Circuits and Syst. (ISCAS), vol. 1, Hong Kong, Jun. 1997, pp. 177-180.

[7] M. Flohberger, W. Kogler, W. Gappmair, and O. Koudelka, "Symbol rate estimation with inverse Fourier transforms," in Proc. Int. Workshop on Satellite and Space Commun., Madrid, Spain, Sep. 2006, pp. 110-113.

[8] H. Xu, Y. Zhou, and Z. Huang, "Blind Roll-Off Factor and Symbol Rate Estimation Using IFFT and Least Squares Estimator," Int. Conf. on Wireless Commun., Networking and Mobile Computing, Sep. 2007, pp. 1052-1055.

[9] Z. Yu, Y.Q. Shi, and W. Su, “Symbol-rate estimation based on filter bank,” in Proc. Int. Symp. on Circuits and Syst,. Kobe, Japan, May 2005, pp. 1437-1440.

[10] L. Mazet and Ph. Loubaton, “Cyclic correlation based symbol rate estimation,” in Proc. Asilomar Conf. Signals, Syst., and Computers, Pacific Grove, CA, Nov. 1999, pp. 1008–1012.

[11] M. Kueckenwaitz, F. Quint, and J. Reichert, , "A robust baud rate estimator for noncooperative demodulation," in Proc. Military Commun. Conf. (MILCOM), vol. 2, Los Angeles, CA, Oct. 2000, pp. 971-975.

[12] S. Tang and Y. Yu, "Fast algorithm for symbol rate estimation", IEICE Trans. on Commun., pp. 1649-1652, 2005.

[13] W.A. Gardner, "Exploitation of spectral redundancy in cyclostationary signals," IEEE Sig. Process. Mag., vol. 8, no. 2, pp. 14-36, Apr. 1991.

[14] ——, "Measurement of spectral correlation," IEEE Trans. on Acoust., Speech and Signal Process., vol. 34, no. 5, pp. 1111-1123, Oct. 1986.

[15] ——, "Signal interception: a unifying theoretical framework for feature detection," IEEE Trans. on Commun., vol. 36, no. 8, pp. 897-906, Aug. 1988.

[16] X. Jun, W. Fu-ping, and W. Zan-ji, "The improvement of symbol rate estimation by the wavelet transform," in Proc. Int. Conf. on Commun., Circuits and Syst, vol. 1, May 2005, pp. 100-103.

[17] W.A. Gardner, "Cyclostationarity in communications and signal processing", IEEE Press, 1994.

[18] A.V. Dandawate and G.B. Giannakis, "Statistical tests for presence of cyclostationarity," IEEE Trans. on Sig. Process, vol. 42, no. 9, pp. 2355-2369, Sep. 1994.

[19] R.S. Roberts, W.A. Brown, and H.H. Loomis Jr. , "Computationally efficient algorithms for cyclic spectral analysis ," IEEE Sig. Process. Mag., vol. 8, no. 2, pp. 38-49, Apr. 1991.

[20] W.A. Brown III and H.H. Loomis Jr., "Digital implementations of spectral correlation analyzers," IEEE Trans. on Sig. Process., vol. 41, no. 2, pp. 703-720, Feb. 1993.

[21] E. Terzi and H. Arslan, "Blind Symbol Rate Estimation: A Two Stage Approach", in Proc. IEEE 17th Sig. Process., Commun. and App. Conf., Antalya, Turkey, Apr. 2009.

[22] P. D. Welch, "The use of fast Fourier transform for the estimation of power spectra: A method based on time averaging over short, modified periodograms," IEEE Trans. Audio Electroacoust., vol. AU-15, no. 2, pp. 70-73, Jun. 1967.

[23] G. L. Stuber, "Principles of Mobile Communication", 2nd ed., Kluwer Academic Publishers, 2002.

[24] B. P. Lathi, "Modern Digital and Analog Communication Systems", 3rd ed., Oxford University Press, 1998.

[25] J.G. Proakis, "Digital Communications", 4th ed., McGraw-Hill, 2000.

[26] J.D. Gibson, "The Mobile Communications Handbook", 1st ed., CRC Press, 1995.

[27] A. Viterbi, "Nonlinear estimation of PSK-modulated carrier phase with application to burst digital transmission," Info. Theory, vol. 29, no. 4, pp. 543-551, July 1983.

[28] Y. Wang, K. Shi, and E. Serpedin, "Non-data-aided feedforward carrier frequency offset estimators for qAM Constellations: a nonlinear least-squares approach," EURASIP Journal on Applied Sig. Process., vol. 2004, no. 13, pp. 1993-2001, 2004.

[29] K.E. Scott and E.B. Olasz, "Simultaneous clock phase and frequency offset estimation," IEEE Trans. on Commun., vol. 43, no. 7, pp. 2263-2270, July 1995.

[30] H. Sari and S. Moridi, "New phase and frequency detectors for carrier recovery in PSK and QAM systems," IEEE Trans. on Commun., vol. 36, no. 9, pp. 1035-1043, Sep 1988.

[31] KY. Kim and HJ. Choi, "Design of carrier recovery algorithm for high-order QAM with large frequency acquisition range," IEEE Int. Conf. on Commun., vol. 4, June 2001, pp. 1016-1020.

[32] Y. Ouyang and CL. Wang, "A New Carrier Recovery Loop for High-Order Quadrature Amplitude Modulation", IEICE Trans. on Commun., pp. 4250-4258, 2005.

[33] Q. Liu, Z. Yang, J. Song and C. Pan, "A novel QAM joint frequency-phase carrier recovery method," The 8th Int. Conf. on Adv. Commun. Tech., vol. 3, Feb. 2006, pp. 5.

[34] A. Swami and B.M. Sadler, "Hierarchical digital modulation classification using cumulants," IEEE Trans. on Communications, vol. 48, no. 3, pp. 416-429, Mar. 2000.

[35] O.A. Dobre, Y. Bar-Ness, and W. Su, "Robust QAM modulation classification algorithm using cyclic cumulants," IEEE Wireless Commun. and Netw. Conf., Mar. 2004, pp. 745-748.

[36] G. Hatzichristos and M.P. Fargues, "A hierarchical approach to the classification of digital modulation types in multipath environments," in Proc. Asilomar Conf. Signals, Syst., and Computers, vol. 2, Nov. 2001, pp. 1494-1498.

[37] D. Grimaldi, S. Rapuano, and L. De Vito, "An Automatic Digital Modulation Classifier for Measurement on Telecommunication Networks," IEEE Trans. on Instrumentation and Measurement, vol. 56, no. 5, pp. 1711-1720, Oct. 2007.

[38] P. Prakasam and M. Madheswaran "Digital Modulation identification model using wavelet transform and statistical parameters", Journal. Comp. Sys., Netw., and Commun., vol. 2008, pp. 1-8, Feb. 2008.

[39] L. Hong and K.C. Ho, "Identification of digital modulation types using the wavelet transform," in Proc. Military Commun. Conf. (MILCOM), vol. 1, Atlantic City, NJ, Oct. 1999, pp. 427-431.